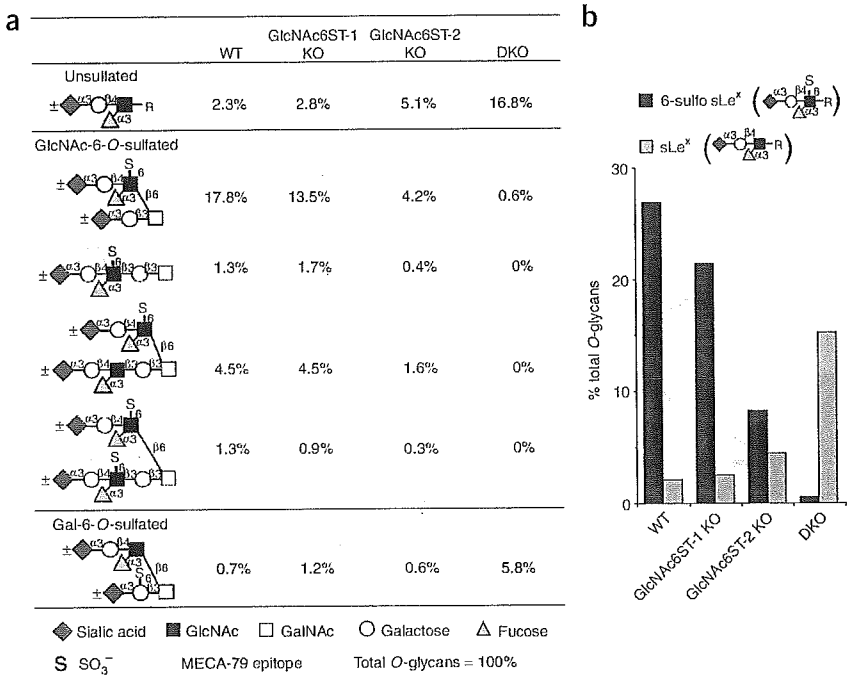

Figure 5 Structures of *O*-glycans attached to GlyCAM-1. **(a)** Fucosylated and/or sulfated *O*-glycans attached to GlyCAM-1 from wild-type and null mice. **(b)** Percentage of *O*-glycans attached to GlyCAM-1 containing 6-sulfo sialyl Lewis X (6-sulfo sLe^x) and unsulfated sialyl Lewis X (sLe^x). Total *O*-glycans attached to GlyCAM-1 = 100%. Data are representative of two independent experiments.

(**Supplementary Fig. 1** online). Sialic acid modification was present at the termini of 89.5%, 87.2%, 87.5% and 90.5% of the oligosaccharides in wild-type, GlcNAc6ST-1-deficient, GlcNAc6ST-2-deficient and double-knockout mice, respectively. Combined with the detailed structural analysis of the desialylated oligosaccharides, these results indicate that the 6-sulfo sialyl Lewis X structure was almost completely abrogated, whereas unsulfated sialyl Lewis X was overexpressed in the double-knockout mice (**Fig. 5b**).

Expression and substrate specificity of sulfotransferases

As shown above, some sulfated *O*-glycans were expressed in double-knockout mice. To determine which sulfotransferases were expressed and were involved in the biosynthesis of sulfated *O*-glycans in HEVs, we next did RT-PCR analysis using total RNA from peripheral lymph node HEV cells of wild-type mice, prepared by immunomagnetic selection with MECA-79 (**Fig. 6a**). After confirming expression of GlyCAM-1 and lack of expression of L-selectin in the MECA-79$^+$ HEV cell preparations, we examined the expression of sulfotransferases in these cell preparations. In addition to GlcNAc6ST-1 and GlcNAc6ST-2, we detected GlcNAc6ST-4 (refs. 26,27). Expression of GlcNAc6ST-3 (ref. 28) was not detectable in these cell preparations, although it was readily detectable in the same conditions in mouse cornea, which is known to express this sulfotransferase[29]. All four mouse GlcNAc6STs efficiently transferred sulfate to core 2–branched *O*-glycans, as shown by [^{35}S]Na_2SO_4 incorporation. In contrast, only GlcNAc6ST-2 and GlcNAc6ST-3 efficiently transferred sulfate to extended core 1 *O*-glycans, resulting in the generation of substantial MECA-79 epitope, as shown by immunoblot (**Fig. 6b**). GlcNAc6ST-1 inefficiently synthesized the MECA-79 epitope, whereas GlcNAc6ST-4 did not synthesize detectable amounts of this epitope, consistent with the finding that the MECA-79 epitope was abolished in the double-knockout mice (**Fig. 2a**). These results combined suggest that the small amount of core 2–branched *O*-glycans containing GlcNAc-6-*O*-sulfate identified in the double-knockout mice were synthesized by GlcNAc6ST-4. We also detected by RT-PCR expression of the galactose-6-*O*-sulfotransferase keratan sulfate sulfotransferase (KSST)[30], which is probably involved in the biosynthesis of the *O*-glycans containing galactose-6-*O*-sulfate identified in our carbohydrate analysis.

Functions of unsulfated sialyl Lewis X

As described above, the main carbohydrate structural changes in the double-knockout mice were the almost complete absence of the 6-sulfo sialyl Lewis X structure and abundant expression of the unsulfated sialyl Lewis X structure. To determine whether the low but detectable L-selectin ligand activity in the double-knockout mice was mediated by the unsulfated sialyl Lewis X structure, we assessed L-sel–IgM binding (**Fig. 6c**). Staining of L-sel–IgM on HEVs was abrogated in frozen sections of peripheral lymph nodes from mice doubly deficient in both FucT-IV and FucT-VII, indicating that fucose modification was critically important for binding of L-sel–IgM to the HEVs of peripheral lymph nodes. In addition, binding of L-sel–IgM to HEVs was abolished by sialidase treatment of frozen sections of peripheral lymph nodes from double-knockout mice, indicating that sialic acid modification was also indispensable. In accordance with those observations, preinjection of the fucose-specific lectin *Aleuria aurantia* agglutinin (AAA), or the α(2,3)-linked sialic acid–specific lectin *Maackia amurensis* agglutinin (MAA) into double-knockout mice inhibited homing of lymphocytes to peripheral lymph nodes by 85.2% or 78.7%, respectively (**Fig. 6d**). These results suggest that the residual L-selectin ligand activity in double-knockout mice was most likely mediated by the abundantly expressed unsulfated sialyl Lewis X structure.

DISCUSSION

We have shown here that GlcNAc6ST-1 and GlcNAc6ST-2 cooperatively have a chief function in the biosynthesis of L-selectin ligand carbohydrates in HEVs. Mutant mice deficient in both sulfotransferases showed substantially lower lymphocyte trafficking to peripheral lymph nodes, as well as less robust inflammatory responses after sensitization and challenge with the hapten DNFB. We also did a systematic carbohydrate structural analysis of a HEV-derived glycoprotein and have provided a structural 'explanation' for the phenotypes of mutant mice.

We have shown here that more than 25% of the total carbohydrates on GlyCAM-1 are modified with the 6-sulfo sialyl Lewis X capping structure on HEVs in wild-type mice, indicating that this carbohydrate structure is indeed a principal capping structure of GlyCAM-1. Carbohydrate structural analysis of double-knockout mice indicated that GlcNAc6ST-1 and GlcNAc6ST-2 are required for biosynthesis of this capping structure. Although we detected another member of the GlcNAc-6-*O*-sulfotransferase family, GlcNAc6ST-4, in MECA-79$^+$ HEV cells, structural analysis indicated

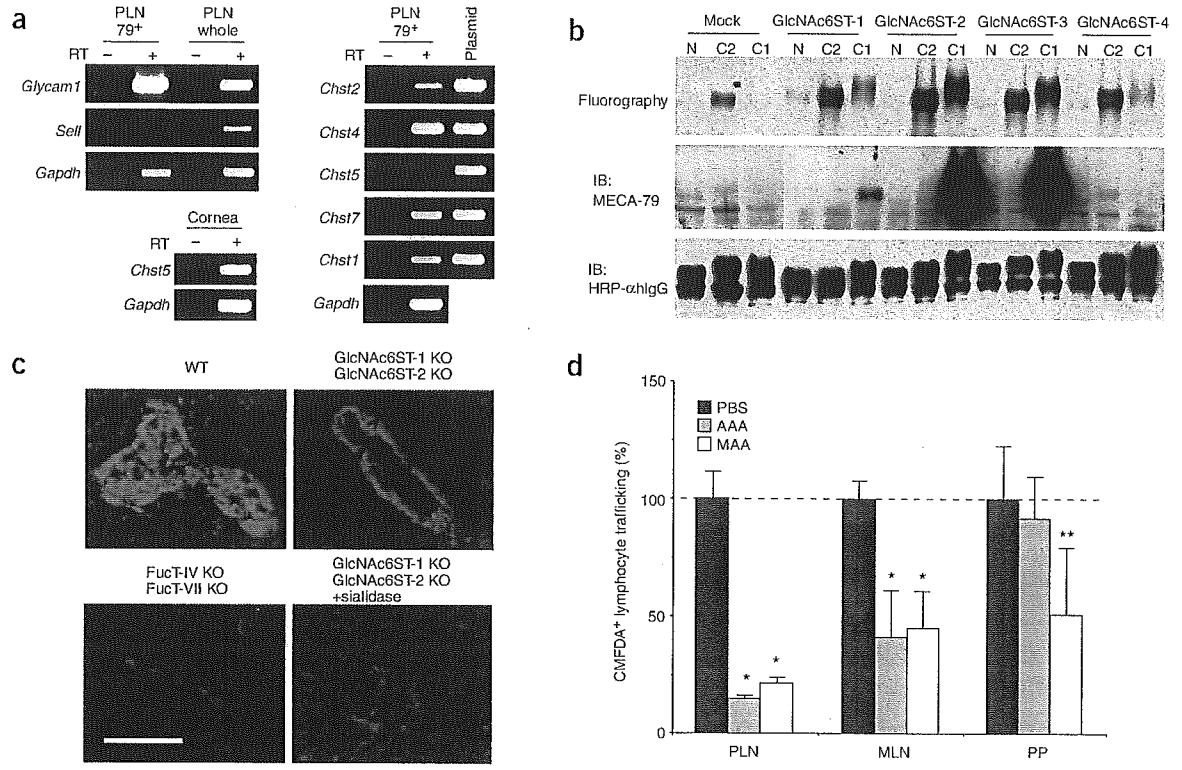

Figure 6 Expression of sulfotransferases in HEVs and characterization of remaining lymphocyte homing in double-knockout mice. **(a)** Expression of sulfotransferase genes. For this PCR, templates were single-stranded cDNAs constructed from MECA-79$^+$ HEVs from peripheral lymph nodes (PLN 79$^+$), whole-cell suspensions from peripheral lymph nodes (PLN whole) or corneas from wild-type mice (Cornea) or plasmid DNA containing full-length sulfotransferase cDNA (Plasmid). PCR was done in the presence (+) or absence (–) of reverse transcriptase (RT). *Chst2*, GlcNAc6ST-1; *Chst4*, GlcNAc6ST-2; *Chst5*, GlcNAc6ST-3; *Chst7*, GlcNAc6ST-4; *Chst1*, KSST; *Glycam1*, GlyCAM-1; *Sell*, L-selectin; *Gapdh*, glyceraldehyde-3-phosphate dehydrogenase. **(b)** Immunoblot of MECA-79. Lec2 cells were transiently transfected with expression vectors encoding GlyCAM-1-IgG without (N) or with Core2GlcNAcT-I (C2) and Core1-β3GlcNAcT (C1), together with nothing else (Mock) or with GlcNAc6ST-1–GlcNAc6ST-4. Cells were metabolically labeled with [^{35}S]Na_2SO_4. GlyCAM-1-IgG was purified with protein A–Sepharose and was analyzed by fluorography and immunoblot (IB) with MECA-79. The amount of GlyCAM-1-IgG was normalized by immunoblot with horseradish peroxidase–labeled antibody to human IgG (HRP-αhIgG). **(c)** Expression of L-selectin ligands. Frozen sections (7 μm in thickness) of peripheral lymph nodes from wild-type and mutant mice pretreated with sialidase (from *Vibrio cholerae*; 200 mU/ml) or not pretreated and stained with L-sel–IgM. Scale bar, 50 μm. **(d)** Trafficking of lymphocytes to lymphoid organs of double-knockout mice. CMFDA-labeled lymphocytes were injected into double-knockout mice 1 h after injection of phosphate-buffered saline (PBS), AAA lectin (100 μg) in PBS, or MAA lectin (40 μg) in PBS. Trafficking is presented as a percentage of that in PBS-injected mice, which was set as 100% ($n = 3$). *, $P < 0.01$, and **, $P < 0.1$, versus PBS-injected mice. Data are representative of three independent experiments.

that it has only a minor function in GlcNAc-6-*O*-sulfation of L-selectin ligands.

Although both GlcNAc6ST-1 and GlcNAc6ST-2 function in the GlcNAc-6-*O*-sulfation of L-selectin ligands, these sulfotransferases showed some differences in relation to L-selectin ligand biosynthesis in HEVs. GlcNAc6ST-2 seemed to be the main GlcNAc-6-*O*-sulfotransferase in peripheral lymph nodes and mesenteric lymph nodes, as staining with MECA-79 and L-sel–IgM binding was greatly diminished in the HEVs of these secondary lymphoid organs in the absence of GlcNAc6ST-2 but not in the absence of GlcNAc6ST-1. Consequently, homing of lymphocytes to these secondary lymphoid organs and the production of 6-sulfo sialyl Lewis X-containing *O*-glycans were more diminished in GlcNAc6ST-2-deficient mice than in GlcNAc6ST-1-deficient mice. Consistent with that finding, GlcNAc6ST-2 was expressed more abundantly in HEVs of peripheral lymph nodes than was GlcNAc6ST-1, as assessed by RT-PCR. In contrast, GlcNAc6ST-1 seemed to be the main GlcNAc-6-*O*-sulfotransferase in Peyer's patches, as MECA-79 antibody staining was abrogated in the absence of GlcNAc6ST-1. In accordance with that result, we found that expression of GlcNAc6ST-2 in Peyer's patches was undetectable, as judged by the fluorescence of the GlcNAc6ST-2–EGFP chimeric protein expressed under control of the promoter of the gene encoding GlcNAc6ST-2 (ref. 17).

Furthermore, GlcNAc6ST-2 seemed to be more relevant in the biosynthesis of fucosylated and sulfated *O*-glycans than GlcNAc6ST-1, because in mice deficient in GlcNAc6ST-2 alone, the percentage of *O*-glycans containing both fucose and sulfate was much lower, whereas the percentage of *O*-glycans containing only GlcNAc-6-*O*-sulfate but not fucose was slightly higher. The different ability in forming fucosylated and sulfated products may be due to the difference in the subcellular localizations of GlcNAc6ST-1 and GlcNAc6ST-2. GlcNAc6ST-1 is confined to the *trans*-Golgi network, whereas GlcNAc6ST-2 is distributed throughout the Golgi apparatus[31]; the latter may be more suitable to supply sulfated *O*-glycan acceptors to FucT-VII, a broadly Golgi-distributed glycosyltransferase[32], although further experimental verification is required to clarify that point.

Moreover, the acceptor substrate specificity of GlcNAc6ST-1 and GlcNAc6ST-2 overlaps but differs. Both sulfotransferases efficiently

transferred sulfate to core 2 *O*-glycans, whereas only GlcNAc6ST-2 efficiently transferred sulfate to extended core 1 *O*-glycans to form the MECA-79 epitope. These results collectively indicate that GlcNAc6ST-2 alone is not sufficient for full formation of 6-sulfo sialyl Lewis X despite its robust expression in HEVs of peripheral lymph nodes. The difference in the substrate specificities and possibly different subcellular localizations of GlcNAc6ST-1 and GlcNAc6ST-2 may contribute to the cooperative actions of these two sulfotransferases in the biosynthesis of L-selectin ligands in HEVs.

The homing of lymphocytes to peripheral lymph nodes in double-knockout mice was almost completely blocked by MEL-14. Although we detected binding of L-sel–IgM only on the lining of HEVs on the surface away from the lumen in double-knockout mice, it is conceivable that L-selectin ligands are weakly expressed on the lumenal surface of HEVs but below the detection level of immunofluorescence. The most likely candidate for supporting residual lymphocyte trafficking to peripheral lymph nodes in double-knockout mice is the unsulfated sialyl Lewis X structure, as it is abundantly expressed in the double-knockout mice and interacts with L-selectin *in vitro*[33]. In agreement with that hypothesis, homing of lymphocytes to peripheral lymph nodes is abolished in mice doubly deficient in both FucT-IV and FucT-VII (ref. 8). Similarly, our immunofluorescence study showed that L-sel–IgM did not bind to lymph node tissue sections of mice doubly deficient in both FucT-IV and FucT-VII. Moreover, preinjection of the fucose- and sialic acid–specific lectins AAA and MAA, respectively, inhibited homing of lymphocytes to peripheral lymph nodes and mesenteric lymph nodes in the double-knockout mice, indicating that both fucose and sialic acid are essential for residual lymphocyte homing in these mice.

Unsulfated sialyl Lewis X structures on extended core 1 as well as core 2–branched *O*-glycans efficiently support L-selectin-mediated lymphocyte rolling when the structures are present on P-selectin glycoprotein ligand 1, which contains sulfated tyrosine residues[34]. It has been reported that the P-selectin glycoprotein ligand 1–like molecule endoglycan, which is modified with the sialyl Lewis X structure and sulfated tyrosine residues, interacts efficiently with L-selectin[35]. It is possible, therefore, that the unsulfated sialyl Lewis X structure expressed in double-knockout mice supports lymphocyte rolling only when it is present on specific glycoproteins, such as endoglycan. However, our results have shown that GlyCAM-1 from double-knockout mice, which lacks tyrosine sulfation, weakly supported lymphocyte rolling, suggesting that abundant expression of unsulfated sialyl Lewis X in double-knockout mice may account at least in part for the residual lymphocyte homing. Indeed, GlyCAM-1 from double-knockout mice supported shear stress–dependent lymphocyte rolling, as expected given the L-selectin-dependent lymphocyte rolling[36]. The number of rolling lymphocytes on GlyCAM-1 from double-knockout mice decreased more than the number of lymphocytes with transient tethers. These results suggest that the rolling velocity is more affected than the initial tethering in double-knockout mice, consistent with the finding that 6-sulfation of sialyl Lewis X substantially decreases the rolling velocity of lymphocytes[13,17,37]. Intravital microscopy has shown the rolling velocity of lymphocytes increases considerably in the double-knockout mice, which results in a substantial reduction in the number of cells sticking on HEVs[38]. That same analysis has also shown that the rolling of B lymphocytes is diminished more substantially in HEVs than in medullary venules, consistent with the finding that rolling in HEVs is more dependent on sulfation than is rolling in medullary venules, as assessed by MECA-79 antigen expression[39]. Along with our carbohydrate structural analysis, those studies suggest that sialyl Lewis X can function as a substitute L-selectin ligand in the absence of 6-sulfo sialyl Lewis X, although the rolling velocity supported by the former is much faster than that supported by the latter.

In addition to the abundant unsulfated sialyl Lewis X in double-knockout mice, we have identified a previously unknown structure containing unsulfated sialyl Lewis X in the core 2 branch and galactose-6-*O*-sulfate in the core 1 branch; this carbohydrate structure represented 5.8% of the total carbohydrates on GlyCAM-1 derived from double-knockout mice. It is possible that this structure is also partially responsible for residual L-selectin ligand activity in these mice, as transfection of cDNA encoding KSST enhances L-selectin ligand activity *in vitro*[14,37]. However, this structure should have minimal involvement in lymphocyte homing, because the substantial increase in its abundance in double-knockout mice was not associated with an increase in lymphocyte homing activity.

Although it has been reported that the 6′-sulfo sialyl Lewis X capping structure (sialyl-α(2-3)-[sulfo-6]-galactopyranosyl-β(1-4)-[fucopyranosyl-α(1-3)]-*N*-acetylglucosaminyl-β1-R) is expressed in HEVs[40], we did not detect this carbohydrate structure in our analysis, possibly because this structure is not efficiently synthesized because of acceptor competition between FucT-VII and KSST. As described before, FucT-VII transfers few if any fucose residues to sialyl lactosamine modified with galactose-6-*O*-sulfate[7]. Conversely, KSST does not transfer sulfate to the galactose residue of the sialyl Lewis X structure[41]. Combined with our carbohydrate analysis, those findings suggest that KSST overexpression may negatively regulate L-selectin ligand activity by competing for acceptor substrates with FucT-VII, as fucosylation by FucT-VII is critically important for the biosynthesis of L-selectin ligands[7]. Preliminary results have indicated that KSST overexpression indeed inhibits sialyl Lewis X expression in FucT-VII transfectants (N.H., H.K. and M.F., unpublished observations). Thus, KSST may function both positively[14,37] and negatively in the biosynthesis of L-selectin ligand carbohydrates, depending on its abundance.

To determine the functions of GlcNAc6ST-1 and GlcNAc6ST-2 in immune responses in pathophysiological conditions, we assessed contact hypersensitivity responses in double-knockout mice and found that these mice had substantially less in ear swelling and leukocyte infiltration than did wild-type mice. We also found that the total number of lymphocytes was greatly reduced in the draining lymph nodes after sensitization with DNFB, although antigen-specific lymphocytes were present in the draining lymph nodes at the same ratio found in wild-type mice. Thus, it is likely that the quantitative reduction in antigen-specific lymphocytes resulted in the overall reduction in the contact hypersensitivity responses in these mice. This reduction occurred only in the double-knockout mice, indicating a critical threshold for the amount of L-selectin ligands to attain normal contact hypersensitivity responses. Our results are reminiscent of the phenotypes of L-selectin-deficient mice[42] and mice doubly deficient in both FucT-IV and FucT-VII (ref. 43), in which contact hypersensitivity responses are impaired due in part to a lack of antigen-specific lymphocytes in the draining lymph nodes. In mice deficient in L-selectin or fucosyltransferase, however, not only homing of naive lymphocytes to the regional lymph nodes but also effector cell trafficking to the inflammatory sites is impaired, because the interaction between L-selectin and sialyl Lewis X–modified P-selectin glycoprotein ligand 1 is completely abolished. In contrast, only the former was impaired in our sulfotransferase double-knockout mice. Thus, we have shown that homing of naive lymphocytes to the regional lymph nodes is actually a key determinant of the contact hypersensitivity response.

HEV-like vessels reactive with MECA-79 are detected in several disorders associated with chronic inflammation[44]. MECA-79-reactive

HEV-like vessels are detected in human gastric mucosa infected by *Helicobacter pylori*[45]. However, the physiological function of the MECA-79 epitope expressed in these specialized blood vessels is unclear, except for the demonstration that MECA-79 has a therapeutic effect in a sheep model of asthma[46]. As double-knockout mice completely lack the MECA-79 epitope, these mice will be useful for assessing the functions of this carbohydrate epitope at sites of chronic inflammation, such as the pancreas and salivary glands of nonobese diabetic mice[47,48], the hyperplastic thymus of AKR mice[49], the inflamed joints of rheumatoid arthritis[50] and the mouse model for inflammation induced by *H. pylori (felis)*[51].

In conclusion, our findings have demonstrated the essential function of GlcNAc6ST-1 and GlcNAc6ST-2 in the biosynthesis of the 6-sulfo sialyl Lewis X structure in HEVs, which serves as a dominant ligand for the lymphocyte-homing receptor L-selectin. Our studies provide a link between carbohydrate structural changes and alterations in trafficking of lymphocytes to secondary lymphoid organs in normal and pathophysiological conditions. As many studies have linked carbohydrates to immune cell recruitment, studies linking carbohydrate structure and function should become increasingly important in this field.

METHODS

Mice. Double-knockout mice were generated by breeding of mice singly deficient in GlcNAc6ST-1 (ref. 23) and GlcNAc6ST-2 (ref. 17). Genomic DNA was isolated from mouse tails and was used for PCR genotyping. For the simultaneous detection of wild-type and mutant alleles encoding GlcNAc6ST-1, primers 5′-TCTATGAGCCTGTGTGGCACGT-3′ (G6W5), 5′-GCATACCACCTTGTTAGTGGC-3′ (G6W3) and 5′-TGACAACGTCGAG CACAGCTG-3′ (NeoP5) were used. For detection of the alleles encoding GlcNAc6ST-2, primers F2W, R2W and R1M were used as described[17]. Mice doubly deficient in both FucT-IV and FucT-VII, generated as described[8], were provided by the Functional Glycomics Consortium (La Jolla, California). Mice were treated in accordance with guidelines of the National Institutes of Health and the United States Department of Agriculture and experiments were approved by the Animal Research Committee of the Burnham Institute (La Jolla, California).

Lymphocyte homing assay. This was done as described[17]. Lymphocytes from spleens and mesenteric lymph nodes of wild-type mice were labeled with chloromethyl fluorescence diacetate (CMFDA) and 2.5×10^7 cells were injected into the tail veins of 7- to 8-week-old wild-type and mutant mice. After 1 h, mice were killed and peripheral lymph nodes, mesenteric lymph nodes and Peyer's patches were collected. Lymphocyte suspensions were prepared from these organs and were analyzed by flow cytometry to determine the fractional content of fluorescent cells.

Lymphocyte rolling assay. GlyCAM-1 was purified from serum obtained from mice of each strain[52]. The concentration of GlyCAM-1 in each preparation was almost equivalent, as assessed by immunoblot with antibody to GlyCAM-1 prepared in a similar way as described[52]. Purified GlyCAM-1 (10 μl; equivalent to the amount of GlyCAM-1 purified from 10 μl of serum) was applied twice (6 h and overnight) or three times (6 h, overnight, and 6 h) in parallel to polystyrene plates coated with antibody to GlyCAM-1 at concentrations of 20 or 50 μg/ml, respectively. Lymphocytes were added to the flow chamber and were analyzed as described[8]. Based on velocity, rolling cells were classified into two groups: rolling lymphocytes that rolled at least two cell diameters for more than 0.5 s below critical velocity, and transiently tethered lymphocytes that had a high rolling velocity near that of free-floating cells with multiple pauses in less than 0.5 s.

Contact hypersensitivity. Contact hypersensitivity responses were measured as described[25]. The dorsal skin of mice was shaved and 25 μl of 0.5% DNFB (Sigma) in acetone/olive oil (4:1, volume/volume) was applied on days 0 and 1. On day 5, the right ear was treated with 20 μl of 0.2% DNFB (10 μl on the side of the pinna) and the left ear was treated with vehicle. Swelling was measured with a thickness gauge before and 24 h after treatment.

Lymphocyte proliferation assay. Single-cell suspensions were prepared from inguinal lymph nodes of mice sensitized with DNFB on days 0 and 1 as described above and were cultured for 40 h in the presence or absence of 2 μg/ml of concanavalin A (Sigma) or 200 μg/ml of DNBS[25] (MP Biomedicals). Cell proliferation was measured with a CellTiter 96AQueous One Solution Proliferation Assay kit (Promega). The absorbance at 490 nm obtained in the absence of concanavalin A or DNBS was subtracted from that obtained in the presence of these agents.

Structural analysis of *O*-glycans attached to GlyCAM-1. Peripheral lymph node and mesenteric lymph node slices were metabolically labeled with 0.5 mCi/ml of [^{3}H]galactose (American Radiolabeled Chemicals) as described[15,17]. GlyCAM-1 was purified from the conditioned medium and its *O*-glycans were analyzed by Bio-Gel P-4 gel filtration (Bio-Rad), QAE-Sephadex A-25 anion-exchange column (Sigma) and HPLC before and after exoglycosidase treatment, as described[13,15,17], except that the elution condition of the Asahipak NH_2-bonded HPLC column was modified. Solvent A (64% acetonitrile and 36% H_2O), solvent B (25 mM NaH_2PO_4 in solvent A) and solvent C (50 mM NaH_2PO_4 in solvent A) were used for HPLC as follows. Monosulfated tetrasaccharide core *O*-glycans were eluted with a linear gradient from 0% to 30% solvent B in solvent A for 10 min; from 30% to 65% for 40 min; and from 65% to 100% for 5 min, followed by 100% solvent B for 5 min. Monosulfated hexasaccharide core *O*-glycans were eluted with a linear gradient from 0% to 40% solvent B in solvent A for 10 min; from 40% to 80% for 40 min; and from 80% to 100% for 5 min, followed by 100% solvent B for 5 min. Disulfated *O*-glycans were eluted with a linear gradient from 0% to 40% solvent C in solvent A for 10 min; from 40% to 80% for 40 min; and from 80% to 100% for 5 min, followed by 100% solvent C for 15 min.

RT-PCR. HEV cells were purified from peripheral lymph nodes of C57BL/6 mice by immunomagnetic selection with MECA-79 (ref. 53). Mouse corneas were excised surgically from C57BL/6 mice. Total RNA was purified from these preparations and was used for RT-PCR as described[13]. Primers used to detect genes encoding mouse GlcNAc6ST-1 and mouse GlcNAc6ST-2 have been described[13]. Primers used to detect genes encoding other molecules were as follows: 5′-TGCTGGTACTGTCCTCGTGG-3′ and 5′-TGATGTTGCCACGAGC GAAGG-3′ for mouse GlcNAc6ST-3; 5′-TCAACCTAAAGGTGGTGCAACT-3′ and 5′-GGTTAAGAAGAAATCAGCGCGT-3′ for mouse GlcNAc6ST-4; 5′-AAG CCCTACAACCTGGATGTG-3′ and 5′-GAGTTGCGCACTGTGCTGTAT-3′ for mouse KSST; 5′-CGGAATTCCCACCATGAAATTCTTCAC-3′ and 5′-CGGGAT CCAGTTCTTCCTCCACTGTC-3′ for mouse GlyCAM-1; 5′-CTCTGCTACA CAGCCTCTTGC-3′ and 5′-AGGCTCACACTGGACCACTTG-3′ for mouse L-selectin; and 5′-CCTGGCCAAGGTCATCCATGACA-3′ and 5′-ATGAGGTCC ACCACCCTGTTGCT-3′ for mouse glyceraldehyde-3-phosphate dehydrogenase.

Transient transfection and metabolic cell labeling. Lec2 cells[54] were transiently transfected with an expression plasmid encoding GlyCAM-1–IgG[13] in combination with those encoding core 2–*N*-acetylglucosaminyltransferase-I (Core2GlcNAcT-I) or core 1–β1,3-*N*-acetylglucosaminyltransferase (Core1-β3GlcNAcT) and one of the four GlcNAc6STs (GlcNAc6ST-1 through GlcNAc6ST-4). Cells were metabolically labeled with [^{35}S]Na_2SO_4 (100 μCi/ml) as described[13,15]. As a control, vectors without inserts were transfected into Lec2 cells. In Lec2 cells, MECA-79 antigen is efficiently synthesized, as Lec2 cells lack Golgi-sialylation[54] and thus core 1 extension does not compete with α2,3-sialylation of core 1 structure (galactopyranosyl-β(1-3)-*N*-acetylgalactosaminyl-α1-serine (or threonine)).

Statistical analysis. Student's *t*-test was used for statistical analysis.

Accession code. BIND (http://bind.ca): 319185.

Note: Supplementary information is available on the Nature Immunology website.

ACKNOWLEDGMENTS

We thank T. Akama, S. Chen and E. Lammar for critical reading of the manuscript, and A. Morse for organizing the manuscript. Supported by the

National Institutes of Health (P01CA71932 to M.F. and J.B.L.; U54 GM62116 to the Functional Glycomics Consortium) and the Uehara Memorial Foundation, Japan (H.K.).

COMPETING INTERESTS STATEMENT

The authors declare that they have no competing financial interests.

Published online at http://www.nature.com/natureimmunology/
Reprints and permissions information is available online at http://npg.nature.com/reprintsandpermissions/

1. Arbonés, M.L. *et al.* Lymphocyte homing and leukocyte rolling and migration are impaired in L-selectin-deficient mice. *Immunity* **1**, 247–260 (1994).
2. Springer, T.A. Traffic signals for lymphocyte recirculation and leukocyte emigration: the multistep paradigm. *Cell* **76**, 301–314 (1994).
3. Butcher, E.C. & Picker, L.J. Lymphocyte homing and homeostasis. *Science* **272**, 60–66 (1996).
4. von Andrian, U.H. & Mempel, T.R. Homing and cellular traffic in lymph nodes. *Nat. Rev. Immunol.* **3**, 867–878 (2003).
5. Ley, K. & Kansas, G.S. Selectins in T-cell recruitment to non-lymphoid tissues and sites of inflammation. *Nat. Rev. Immunol.* **4**, 325–335 (2004).
6. Rosen, S.D. Ligands for L-selectin: homing, inflammation, and beyond. *Annu. Rev. Immunol.* **22**, 129–156 (2004).
7. Maly, P. *et al.* The α(1,3)fucosyltransferase Fuc-TVII controls leukocyte trafficking through an essential role in L-, E-, and P-selectin ligand biosynthesis. *Cell* **86**, 643–653 (1996).
8. Homeister, J.W. *et al.* The α(1,3) fucosyltransferases FucT-IV and FucT-VII exert collaborative control over selectin-dependent leukocyte recruitment and lymphocyte homing. *Immunity* **15**, 115–126 (2001).
9. Rosen, S.D., Singer, M.S. & Yednock, T.A. Involvement of sialic acid on endothelial cells in organ-specific lymphocyte recirculation. *Science* **228**, 1005–1007 (1985).
10. Imai, Y., Lasky, L.A. & Rosen, S.D. Sulphation requirement for GlyCAM-1, an endothelial ligand for L-selectin. *Nature* **361**, 555–557 (1993).
11. Hemmerich, S., Butcher, E.C. & Rosen, S.D. Sulfation-dependent recognition of high endothelial venules (HEV)-ligands by L-selectin and MECA-79, an adhesion-blocking monoclonal antibody. *J. Exp. Med.* **180**, 2219–2226 (1994).
12. Mitsuoka, C. *et al.* Identification of a major carbohydrate capping group of the L-selectin ligand on high endothelial venules in human lymph nodes as 6-sulfo sialyl Lewis X. *J. Biol. Chem.* **273**, 11225–11233 (1998).
13. Hiraoka, N. *et al.* A novel, high endothelial venule-specific sulfotransferase expresses 6-sulfo sialyl Lewis^x, an L-selectin ligand displayed by CD34. *Immunity* **11**, 79–89 (1999).
14. Bistrup, A. *et al.* Sulfotransferases of two specificities function in the reconstitution of high endothelial cell ligands for L-selectin. *J. Cell Biol.* **145**, 899–910 (1999).
15. Yeh, J.-C. *et al.* Novel sulfated lymphocyte homing receptors and their control by a core1 extension β1,3-*N*-acetylglucosaminyltransferase. *Cell* **105**, 957–969 (2001).
16. Streeter, P.R., Rouse, B.T.N. & Butcher, E.C. Immunohistologic and functional characterization of a vascular addressin involved in lymphocyte homing into peripheral lymph nodes. *J. Cell Biol.* **107**, 1853–1862 (1988).
17. Hiraoka, N. *et al.* Core 2 branching β1,6-*N*-acetylglucosaminyltransferase and high endothelial venule-restricted sulfotransferase collaboratively control lymphocyte homing. *J. Biol. Chem.* **279**, 3058–3067 (2004).
18. Hemmerich, S. *et al.* Sulfation of L-selectin ligands by an HEV-restricted sulfotransferase regulates lymphocyte homing to lymph nodes. *Immunity* **15**, 237–247 (2001).
19. Fukuda, M., Hiraoka, N., Akama, T.O. & Fukuda, M.N. Carbohydrate-modifying sulfotransferases: structure, function and pathophysiology. *J. Biol. Chem.* **276**, 47747–47750 (2001).
20. Hemmerich, S. *et al.* Chromosomal localization and genomic organization for the galactose/*N*-acetylgalactosamine/*N*-acetylglucosamine 6-*O*-sulfotransferase gene family. *Glycobiology* **11**, 75–87 (2001).
21. Uchimura, K. *et al.* Molecular cloning and characterization of an *N*-acetylglucosamine-6-*O*-sulfotransferase. *J. Biol. Chem.* **273**, 22577–22583 (1998).
22. Kimura, N. *et al.* Reconstitution of functional L-selectin ligands on a cultured human endothelial cell line by cotransfection of α1–3 fucosyltransferase VII and newly cloned GlcNAcβ:6-sulfotransferase cDNA. *Proc. Natl. Acad. Sci. USA* **96**, 4530–4535 (1999).
23. Uchimura, K. *et al.* *N*-Acetylglucosamine 6-*O*-sulfotransferase-1 regulates expression of L-selectin ligands and lymphocyte homing. *J. Biol. Chem.* **279**, 35001–35008 (2004).
24. Berlin, C. *et al.* $\alpha_4\beta_7$ integrin mediates lymphocyte binding to the mucosal vascular addressin MAdCAM-1. *Cell* **74**, 185–195 (1993).
25. Phanuphak, P., Moorhead, J.W. & Claman, H.N. Tolerance and contact sensitivity to DNFB in mice. I. *In vivo* detection by ear swelling and correlation with *in vitro* cell stimulation. *J. Immunol.* **112**, 115–123 (1974).
26. Uchimura, K. *et al.* Diversity of *N*-acetylglucosamine-6-*O*-sulfotransferases: molecular cloning of a novel enzyme with different distribution and specificities. *Biochem. Biophys. Res. Commun.* **274**, 291–296 (2000).
27. Bhakta, S. *et al.* Sulfation of *N*-acetylglucosamine by chondroitin 6-sulfotransferase 2 (GST-5). *J. Biol. Chem.* **275**, 40226–40234 (2000).
28. Lee, J.K., Bhakta, S., Rosen, S.D. & Hemmerich, S. Cloning and characterization of a mammalian *N*-acetylglucosamine-6-sulfotransferase that is highly restricted to intestinal tissue. *Biochem. Biophys. Res. Commun.* **263**, 543–549 (1999).
29. Akama, T.O. *et al.* Human corneal GlcNAc 6-*O*-sulfotransferase and mouse intestinal GlcNAc 6-*O*-sulfotransferase both produce keratan sulfate. *J. Biol. Chem.* **276**, 16271–16278 (2001).
30. Fukuta, M. *et al.* Molecular cloning and characterization of human keratan sulfate Gal-6-sulfotransferase. *J. Biol. Chem.* **272**, 32321–32328 (1997).
31. de Graffenried, C.L. & Bertozzi, C.R. Golgi localization of carbohydrate sulfotransferases is a determinant of L-selectin ligand biosynthesis. *J. Biol. Chem.* **278**, 40282–40295 (2003).
32. Zerfaoui, M. *et al.* The cytosolic and transmembrane domains of the β1,6 *N*-acetylglucosaminyltransferase (C2GnT) function as a *cis* to *medial*/Golgi-targeting determinant. *Glycobiology* **12**, 15–24 (2002).
33. Foxall, C. *et al.* The three members of the selectin receptor family recognize a common carbohydrate epitope, the sialyl Lewis^x oligosaccharide. *J. Cell Biol.* **117**, 895–902 (1992).
34. Mitoma, J. *et al.* Extended core 1 and core 2 branched *O*-glycans differentially modulate sialyl Lewis x-type L-selectin ligand activity. *J. Biol. Chem.* **278**, 9953–9961 (2003).
35. Fieger, C.B., Sassetti, C.M. & Rosen, S.D. Endoglycan, a member of the CD34 family, functions as an L-selectin ligand through modification with tyrosine sulfation and sialyl Lewis x. *J. Biol. Chem.* **278**, 27390–27398 (2003).
36. Finger, E.B. *et al.* Adhesion through L-selectin requires a threshold hydrodynamic shear. *Nature* **379**, 266–269 (1996).
37. Tangemann, K., Bistrup, A., Hemmerich, S. & Rosen, S.D. Sulfation of a high endothelial venule-expressed ligand for L-selectin: effects on tethering and rolling of lymphocytes. *J. Exp. Med.* **190**, 935–941 (1999).
38. Uchimura, K. *et al.* A major class of L-selectin ligands is eliminated in mice deficient in two sulfotransferases expressed in high endothelial venules. *Nat. Immunol.* advance online publication 9 October 2005(doi:1038/ni 1258).
39. M'Rini, C. *et al.* A Novel endothelial L-selectin ligand activity in lymph node medulla that is regulated by α(1,3)-fucosyltransferase-IV. *J. Exp. Med.* **198**, 1301–1312 (2003).
40. Hemmerich, S., Leffler, H. & Rosen, S.D. Structure of the *O*-glycans in GlyCAM-1, an endothelial-derived ligand for L-selectin. *J. Biol. Chem.* **270**, 12035–12047 (1995).
41. Torii, T., Fukuta, M. & Habuchi, O. Sulfation of sialyl *N*-acetyllactosamine oligosaccharides and fetuin oligosaccharides by keratan sulfate Gal-6-sulfotransferase. *Glycobiology* **10**, 203–211 (2000).
42. Catalina, M.D. *et al.* The route of antigen entry determines the requirement for L-selectin during immune responses. *J. Exp. Med.* **184**, 2341–2351 (1996).
43. Smithson, G. *et al.* Fuc-TVII is required for T helper 1 and T cytotoxic 1 lymphocyte selectin ligand expression and recruitment in inflammation, and together with Fuc-TIV regulates naive T cell trafficking to lymph nodes. *J. Exp. Med.* **194**, 601–614 (2001).
44. Rosen, S.D. Endothelial ligands for L-selectin. From lymphocyte recirculation to allograft rejection. *Am. J. Pathol.* **155**, 1013–1020 (1999).
45. Kobayashi, M. *et al.* Induction of peripheral lymph node addressin in human gastric mucosa infected by *Helicobacter pylori*. *Proc. Natl. Acad. Sci. USA* **101**, 17807–17812 (2004).
46. Rosen, S.D., Tsay, D., Singer, M.S., Hemmerich, S. & Abraham, W.M. Therapeutic targeting of endothelial ligands for L-selectin (PNAd) in a sheep model of asthma. *Am. J. Pathol.* **166**, 935–944 (2005).
47. Hanninen, A. *et al.* Vascular addressins are induced on islet vessels during insulitis in nonobese diabetic mice and are involved in lymphoid cell binding to islet endothelium. *J. Clin. Invest.* **92**, 2509–2515 (1993).
48. Faveeuw, C., Gagnerault, M-C. & Lepault, F. Expression of homing and adhesion molecules in infiltrated islets of Langerhans and salivary glands of nonobese diabetic mice. *J. Immunol.* **152**, 5969–5978 (1994).
49. Michie, S.A., Streeter, P.R., Butcher, E.C. & Rouse, R.V. L-selectin and $\alpha_4\beta_7$ integrin homing receptor pathways mediate peripheral lymphocyte traffic to AKR mouse hyperplastic thymus. *Am. J. Pathol.* **147**, 412–421 (1995).
50. Michie, S.A., Streeter, P.R., Bolt, P.A., Butcher, E.C. & : Picker, L.J. The human peripheral lymph node vascular addressin. An inducible endothelial antigen involved in lymphocyte homing. *Am. J. Pathol.* **143**, 1688–1698 (1993).
51. Fox, J.G. *et al.* Hypertrophic gastropathy in *Helicobacter felis*-infected wild-type C57BL/6 mice and p53 hemizygous transgenic mice. *Gastroenterology* **110**, 155–166 (1996).
52. Singer, M.S. & Rosen, S.D. Purification and quantification of L-selectin-reactive GlyCAM-1 from mouse serum. *J. Immunol. Methods* **196**, 153–161 (1996).
53. Girard, J.P. & Springer, T.A. Cloning from purified high endothelial venule cells of hevin, a close relative of the antiadhesive extracellular matrix protein SPARC. *Immunity* **2**, 113–123 (1995).
54. Deutscher, S.L., Nuwayhid, N., Stanley, P., Briles, E.I. & Hirschberg, C.B. Translocation across Golgi vesicle membranes: a CHO glycosylation mutant deficient in CMP-sialic acid transport. *Cell* **39**, 295–299 (1984).

Clinical utility of quantitative RT-PCR targeted to α1,4-*N*-acetylglucosaminyltransferase mRNA for detection of pancreatic cancer

Satoshi Ishizone,[1] Kazuyoshi Yamauchi,[2] Shigeyuki Kawa,[3] Takefumi Suzuki,[2] Fumiaki Shimizu,[1] Oi Harada,[4] Atsushi Sugiyama,[1] Shinichi Miyagawa,[1] Minoru Fukuda[6] and Jun Nakayama[4,5,7]

Departments of [1]Surgery, [2]Laboratory Medicine, [3]Internal Medicine and [4]Pathology, Shinshu University School of Medicine; [5]Institute of Organ Transplants, Reconstructive Medicine and Tissue Engineering, Shinshu University Graduate School of Medicine, Asahi 3-1-1, Matsumoto 390-8621, Japan; and [6]Glycobiology Program, Cancer Research Center, Burnham Institute for Medical Research, 10901 North Torrey Pines Road, La Jolla, CA 92037, USA

(Received August 29, 2005/Revised October 30, 2005/Accepted November 3, 2005/Online publication January 23, 2006)

α1,4-*N*-Acetylglucosaminyltransferase (α4GnT) is a glycosyltransferase responsible for the biosynthesis of α1,4-GlcNAc-capped *O*-glycans, and is frequently expressed in pancreatic cancer cells but not peripheral blood cells. In the present study, we tested the clinical utility of α4GnT mRNA expressed in the mononuclear cell fraction of peripheral blood as a biomarker of pancreatic cancer. Total RNA isolated from the peripheral blood mononuclear cells from 55 pancreatic cancer patients, 10 chronic pancreatitis patients, and 70 cancer-free volunteers was analyzed quantitatively by reverse transcription-polymerase chain reaction with primers specific for α4GnT, and the expression level of α4GnT mRNA relative to that of glyceraldehyde-3-phosphate dehydrogenase (GAPDH) was measured. When the ratio of α4GnT to GAPDH transcripts exceeded a defined cut-off value, patients were considered to have pancreatic cancer. By these standards, 76.4% of the pancreatic cancer patients were detected by this assay. A strong correlation was obtained between positivity in this assay and the expression of α4GnT protein detected immunohistochemically in pancreatic cancer tissues resected subsequently, suggesting that α4GnT mRNA detected in the peripheral blood is derived from circulating pancreatic cancer cells. Although increased levels of α4GnT mRNA was detected in 40.0% of chronic pancreatitis patients and 17.1% of cancer-free volunteers, the expression levels were significantly lower than those seen in pancreatic cancer patients. These results suggest that quantitative analysis of α4GnT mRNA expressed in the mononuclear cell fraction of peripheral blood will contribute to the detection of pancreatic cancer. (*Cancer Sci* 2006; 97: 119–126)

Pancreatic cancer is one of the most intractable malignancies.[1,2] In particular, the 5-year survival rate of this neoplasm is the lowest of all types of cancer, and it is the fifth leading cause of cancer death in Japan.[3] The poor prognosis of pancreatic cancer is largely attributable to the difficulty in diagnosis of the disease at relatively early stages as well as the highly invasive character of the cancer cells, regardless of the tumor size. In fact, the vast majority of pancreatic cancer patients are diagnosed at advanced stages associated with clinical manifestations such as jaundice and back pain, likely due to the limitation of tumor markers available for the diagnosis of pancreatic cancer at potentially curable stages.[4] Several well-established biomarkers, including CEA,[5] CA19-9,[6] DU-PAN-2[7,8] and Span-1,[9] are available for the detection of pancreatic cancer, but it is also true that these biomarkers are not elevated in certain numbers of pancreatic cancer patients. Thus, in order to detect pancreatic cancer more efficiently, it is necessary to identify novel biomarkers that will be useful for its diagnosis.[10,11]

Mucous glycoproteins secreted from the gastroduodenal mucosa are heavily glycosylated and protect the mucosa against various pathogens and physical stresses. Among the oligosaccharides found in human gastrointestinal mucins, α1,4-GlcNAc-capped *O*-glycan is unique because its expression in normal tissues is limited to gastric gland mucous cells, Brunner's gland of the duodenal mucosa and accessory gland of the pancreaticobiliary tract.[12] Interestingly, this unique *O*-glycan is expressed frequently in neoplastic cells such as carcinomas of the stomach, bile duct and pancreas, as well as pancreatic intraepithelial neoplasia (PanIN-I, PanIN-II and PanIN-III),[13] thus it is regarded as a tumor-associated carbohydrate antigen for these tumors.[12] Recently we isolated a cDNA encoding human α4GnT, which is responsible for the biosynthesis of α1,4-GlcNAc-capped *O*-glycans, by expression cloning from a gastric mucosa cDNA library.[14] We subsequently demonstrated that α4GnT is expressed in the Golgi of gastric gland mucous cells and Brunner's glands in normal gastroduodenal mucosa as well as the Golgi of adenocarcinoma cells such as gastric, pancreatic and biliary tract cancers expressing α1,4-GlcNAc-capped *O*-glycans.[15–17]

Our previous study demonstrated that neither α4GnT RNA nor protein is detectable in the normal peripheral blood cells.[17] Thus, we quantitatively measured the expression levels of α4GnT mRNA in the mononuclear cell fraction of peripheral blood obtained from gastric cancer patients using RT-PCR and demonstrated that this assay is useful to detect, as well as monitor, gastric cancer.[17] The present study extends this assay for detection of pancreatic cancer using a technically

[7]To whom correspondence should be addressed. E-mail: jun@hsp.md.shinshu-u.ac.jp

Abbreviations: α4GnT, α1,4-*N*-Acetylglucosaminyltransferase; GAPDH, glyceraldehyde-3-phosphate dehydrogenase; H. pylori, Helicobacter pylori; MTC, multiple tissue cDNA; ROC, receiver operating characteristic; RT-PCR, reverse transcription–polymerase chain reaction; TAMURA, 3′-6-carboxy-*N*,*N*,*N*′,*N*′-tetramethylrhodamine; TBS, Tris buffered saline.

doi: 10.1111/j.1349-7006.2006.00148.x

improved modification. Specifically, levels of α4GnT mRNA in the mononuclear cell fraction of peripheral blood from pancreatic cancer patients were determined quantitatively using multiplex PCR employed to detect simultaneously both α4GnT and an internal standard gene in a single reaction tube.

Materials and Methods

Clinical samples

The present study involved 55 pancreatic cancer patients (34 men and 21 women; age range 45–92 years [mean ± SE, 68.5 ± 9.8 years]). For the reduction of jaundice, a drainage tube was placed in the common bile duct of 16 of 32 patients whose tumors were located in the pancreatic head, whereas none of the 23 patients whose tumor was located in the body or tail of the pancreas received such drainage. In addition to the pancreatic cancer patients, samples from 10 chronic pancreatitis patients (10 men; ages ranging from 55 to 75 years [65.8 ± 7.6]) and 70 volunteers (70 men; ages ranging from 31 to 90 years [69.4 ± 1.4]) were analyzed. These volunteers underwent a health screening and were verified to be cancer-free by routine examinations including abdominal ultrasonography. Written informed consent was obtained from all patients and volunteers prior to the study. Peripheral blood samples were taken from patients and volunteers. In pancreatic cancer patients, blood samples were collected before surgical resection of the primary tumor. When patients underwent endoscopic biopsy of the gastric mucosa, blood samples were taken minimally at 2-week intervals after biopsy.

In addition to the patients' samples, the Human Blood Fractions MTC Panel of the first-strand cDNA (Clontech, Palo Alto, CA, USA) was analyzed. This panel is composed of mononuclear cells (B cells, T cells and monocytes) pooled from 50 male or female Caucasians, resting $CD8^+$ cells pooled from 33 male or female Caucasians, resting $CD4^+$ cells pooled from 20 male or female Caucasians, resting $CD14^+$ cells pooled from 36 male or female Caucasians, resting $CD19^+$ cells pooled from 34 male or female Caucasians, $CD19^+$ cells activated with pokeweed mitogen pooled from four male or female Caucasians, mononuclear cells activated with pokeweed mitogen and concanavalin A pooled from four male or female Caucasians, $CD4^+$ cells activated with concanavalin A pooled from 12 male or female Caucasians, and $CD8^+$ cells activated with phytohemagglutinin pooled from eight male or female Caucasians. These samples were analyzed using a real-time quantitative RT-PCR assay. In parallel, tissue specimens of pancreatic cancer obtained from 23 patients who subsequently underwent surgical operation for removal of primary tumors were examined by immunohistochemistry, and the tumor stage was classified according to the tumor node metastasis classification system.[18] In addition, pancreatic tissue specimens of two cases operated for chronic pancreatitis were archived from the pathology files of Shinshu University Hospital, Matsumoto, Japan. The study protocol was approved by the Institutional Review Board of Shinshu University School of Medicine.

RNA extraction and cDNA synthesis

Five milliliters of peripheral blood was collected, treated with ethylene diamine tetraacetic acid to prevent coagulation, and layered on 3 mL of Lymphprep (Nycomed Pharma, Oslo, Norway) in a 15-mL polypropylene tube. The tube was centrifuged at 2000*g* for 30 min at 20°C. The mononuclear cell fraction was transferred to a new tube, resuspended in 5 mL phosphate-buffered saline, and then centrifuged at 3000*g* for 5 min. Total RNA was isolated from the pellet using a RNeasy Mini kit (Qiagen, Valencia, CA, USA), followed by DNaseI treatment. After inactivation of DNaseI, 11 μL of the DNaseI-treated RNA was incubated with 1 μL of 10 mM dNTPs and 1 μL of 0.5 mg/mL oligo$(dT)_{15}$ primer (Promega, Madison, WI, USA) at 65°C for 5 min. After chilling on ice, these mixed samples were then incubated with 4 μL of 5× first strand buffer, 1 μL of 0.1 M dithiothreitol, 1 μL of RNase inhibitor (Promega), and 1 μL of the reverse transcriptase SuperScript 2 (Invitrogen, Carlsbad, CA, USA) at 42°C for 1 h. The reaction was terminated by heating at 70°C for 15 min, and samples were then kept at −20°C until real-time quantitative RT-PCR analysis.

Real-time RT-PCR

Quantitation of α4GnT mRNA expressed in peripheral blood mononuclear cells as well as the Human Blood Fractions MTC Panel was carried out using an ABI PRISM 7700 Sequence Detection System (PE Applied Biosystems, Foster City, CA, USA) as described previously, with minor modifications.[17] On the basis of the published human *α4GnT* sequence,[14] specific primer pairs and probes were designed using the Primer Express program (PE Applied Biosystems). Forward and reverse primers for human *α4GnT* were 5′-GTTTTCCTCTTCCC-TTTGGATATGA-3′ (nucleotides +340 to +364; the first nucleotide of the initiation methionine codon is +1) and 5′-AGCTGATGTGGAGCCAGTTTCT-3′ (nucleotides +427 to +448), respectively. These primers were designed to hybridize to different exons of the *α4GnT* gene to avoid amplifying genomic DNA. The TaqMan probe was synthesized as 5′-TGGTACAATCAAATCAACGCCAGCGC-3′ (nucleotides +397 to +422) by PE Applied Biosystems, and it carried a 5′-6-carboxyfluorescein reporter label and a TAMURA quencher group. To normalize α4GnT mRNA expression levels, a housekeeping gene, *GAPDH*, was quantitatively analyzed simultaneously as a control. To construct a standard curve, 10-fold dilutions of the plasmid cDNA harboring *α4GnT* (pcDNAI-α4GnT) ranging from 3×10^{-2} to 3×10^{-10} μg/mL, corresponding to 5×10^9 to 5×10^1 copies/mL were prepared. Similarly, a 10-fold dilution of the plasmid cDNA harboring a partial cDNA sequence of *GAPDH* (pCR2.1-GAPDH), which was constructed as described previously,[17] was prepared from 2.3×10^{-2} to 2.3×10^{-10} μg/mL, corresponding to 5×10^9 to 5×10^1 copies/mL.

Multiplex PCR was carried out in 50 μL of reaction mixture containing 3 μL of cDNA sample, 25 μL of 1× Universal PCR Master Mix (PE Applied Biosystems), 800 nM of the primer set for α4GnT, 80 nM of the primer for *GAPDH*, 125 nM of the TaqMan probe for *α4GnT*, and 100 nM of the TaqMan probe for *GAPDH* that carries the 5′-VIC reporter label and 3′-TAMURA quencher group (PE Applied Biosystems). Reaction tubes were placed in the ABI PRISM 7700 Sequence Analyzer, preheated at 95°C for 10 min and amplified for 50 cycles of 95°C for 15 s, followed by 60°C for 1 min. The abundance of α4GnT mRNA and GAPDH mRNA was determined by comparison with the standard curves for

doi: 10.1111/j.1349-7006.2006.00148.x

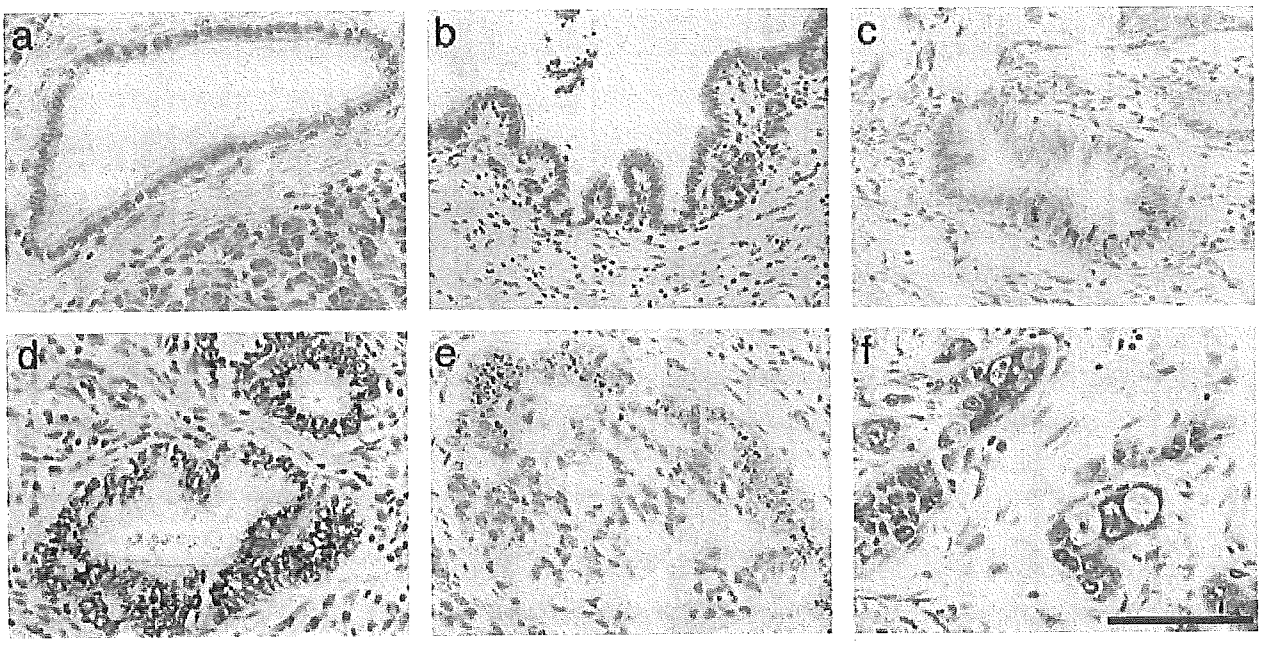

Fig. 1. Expression of α4GnT protein in the normal and neoplastic pancreatic tissues. α4GnT was detected by immunohistochemistry using the antiα4GnT antibody I17K. α4GnT is not expressed in the normal pancreatic duct (a), whereas it is expressed in the Golgi region of pancreatic ducts exhibiting PanIN-IB (b). The α4GnT protein is also expressed in the pancreatic ducts with PanIN-II found in chronic pancreatitis (c). In the pancreatic carcinoma, α4GnT protein is detected in well differentiated (d), moderately differentiated (e), and poorly differentiated (f) adenocarcinomas. Scale bar = 100 μM.

α4GnT and GAPDH, respectively, and the relative expression level of α4GnT mRNA was defined by multiplying the α4GnT : GAPDH mRNA ratio by 1.0×10^7. The assays were carried out in duplicate, and mean values of the two experiments were indicated.

Immunohistochemistry

To detect α4GnT protein in pancreatic cancer cells, 23 cases of the resected pancreatic cancer tissues were subjected to immunohistochemistry with the monospecific antiα4GnT polyclonal antibody, I17K, as described previously.[16] Briefly, 3 μM-thick sections were deparaffinized and treated with 0.3% H_2O_2 in methanol and then blocked with 1% normal goat serum in TBS. The sections were incubated with the antibody for 1.5 h. After washing with TBS, sections were incubated with biotinylated antirabbit IgG and then horseradish peroxidase-labeled streptavidin. The peroxidase reaction was developed with a diaminobenzidine/H_2O_2 solution, and counterstained with hematoxylin. In control experiments carried out by replacing the primary antibody with preimmune serum or omitting the primary antibody from the staining procedure, no specific staining was seen. Tissue specimens containing > 5% positively stained cancer cells were defined as positive, and the others were classified as negative according to previously described criteria.[19]

Enzyme immunoassay of biomarkers in patients' serum

Various biomarkers, including CEA, CA19-9, DU-PAN-2 and Span-1, in pancreatic cancer patients' serum were evaluated by enzyme immunoassay before surgery. CEA (cut-off value, 2.5 ng/mL) was measured using a CEA•Dainapack kit (Dainabot, Tokyo, Japan), and CA19-9 (cut-off value, 37 U/mL) was measured using an AxSYM CA19-9•Dainapack kit (Dainabot). DU-PAN-2 (cutoff value, 150 U/mL) and Span-1 (cutoff value, 30 U/mL) were measured by SRL at Tokyo, Japan.

Statistics

Statistical analyses comparing two independent groups categorized by the clinicopathological variables of pancreatic cancer were carried out using the Mann–Whitney *U*-test. Similarly, comparisons among more than three groups were carried out using the Kruskal–Wallis test. These analyses were performed using StatView 5.0 software (Abacus Concepts, Berkeley, CA, USA). In addition, a cut-off value was determined by constructing a ROC curve using StatMate III (ATMS, Tokyo, Japan). Statistical association between the expression of α4GnT protein in the resected pancreatic cancer tissues and the expression level of α4GnT mRNA determined in the mononuclear cell fraction of peripheral blood was evaluated using Fisher's test (Abacus Concepts). In these analyses, *P*-values < 0.05 were considered to be statistically significant.

Results

Expression of α4GnT protein in pancreatic cancer cells

In order to determine the expression of α4GnT protein in pancreatic ductal adenocarcinoma cells, immunohistochemistry using the antiα4GnT antibody I17K was undertaken with normal and neoplastic tissues of the pancreas, which were resected surgically at the time of operation. In the normal pancreas, α4GnT was not detected in the main or interlobular pancreatic ducts (Fig. 1a). By contrast, α4GnT protein was

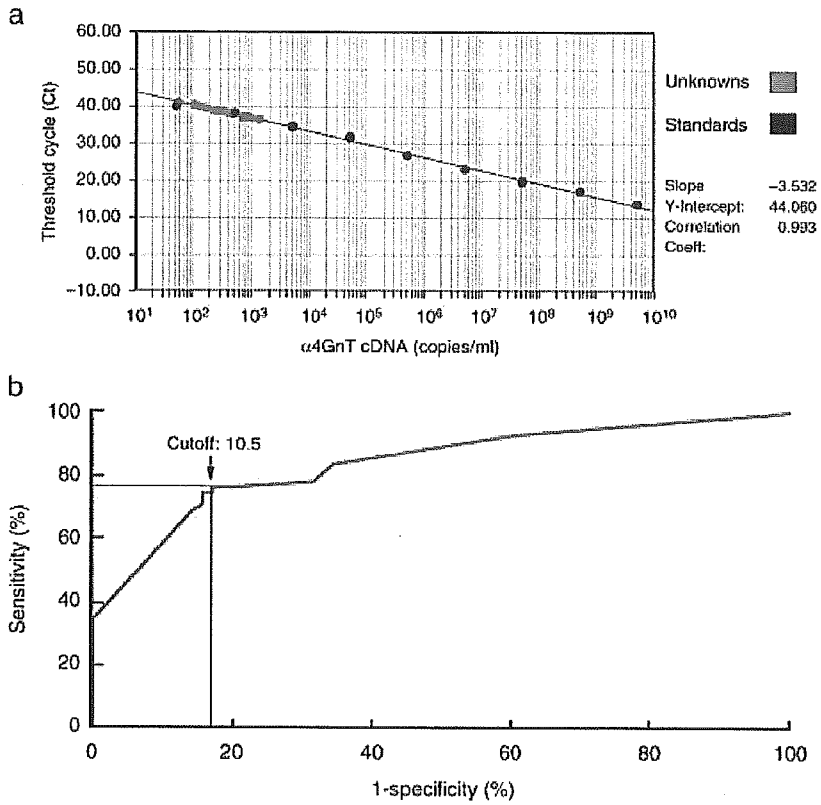

Fig. 2. Quantitative RT-PCR assay targeting α4GnT mRNA. (a) A standard curve for α4GnT was constructed by plotting serially diluted α4GnT cDNA, pcDNAI-α4GnT (black dots), where unknown samples from patients or cancer-free volunteers are indicated as red dots. (b) ROC curve was created by plotting the expression level of α4GnT mRNA in the peripheral blood from 55 pancreatic cancer patients and 70 cancer-free volunteers. Arrow denotes the cutoff value of 10.5, which best discriminates pancreatic cancer patients from cancer-free volunteers with 76.4% sensitivity and 82.9% specificity.

associated with the Golgi region of pancreatic ducts with PanIN-IB (Fig. 1b). α4GnT protein was also expressed in the pancreatic ducts with PanIN-II found in the inflammatory lesions of chronic pancreatitis in both of the two cases examined (Fig. 1c). In pancreatic cancer, α4GnT was detected in the Golgi of adenocarcinoma cells in 73.9% of 23 patients, irrespective of histological tumor type; that is, five of nine patients with well-differentiated adenocarcinoma (Fig. 1d), seven of eight patients with moderately differentiated adenocarcinoma (Fig. 1e) and five of six patients with poorly differentiated adenocarcinoma (Fig. 1f) were positive for α4GnT protein in cancer tissues.

Construction of a standard curve for the quantitative RT-PCR assay

The standard curve for α4GnT mRNA was constructed using 10-fold dilutions of α4GnT cDNA, pcDNAI-α4GnT (Fig. 2a). By defining the cycle number where fluorescence reached a detection threshold as Ct, we obtained a strong linear relationship between Ct and the log of the cDNA concentration. Based on the standard curve, levels of α4GnT mDNA ranging from 5×10^1 to 5×10^9 copies/mL were detected in a reaction tube. Similarly, GAPDH mRNA was detected ranging from 5×10^1 to 5×10^9 copies/mL based on the standard curve for GAPDH constructed using 10-fold dilutions of pCR2.1-GAPDH. Using these standard curves, the expression level of α4GnT mRNA relative to that of GAPDH mRNA was determined.

Determination of a cut-off value distinguishing pancreatic cancer patients from cancer-free volunteers

To most efficiently discriminate pancreatic cancer patients from cancer-free volunteers, a ROC curve was constructed (Fig. 2b). Thus, the α4GnT:GAPDH mRNA ratios multiplied by 1.0×10^7 were defined as the expression level of α4GnT, and the values determined in the mononuclear cell fraction of the peripheral blood from 55 patients with pancreatic cancer versus 70 cancer-free volunteers were plotted. By defining the cut-off value as 10.5, the optimal combination of 76.4% for sensitivity and 82.9% for specificity was obtained. Thus, we regarded a value as positive when expression levels of α4GnT mRNA greater than 10.5 were obtained in this assay.

Determination of the expression levels of α4GnT mRNA in peripheral blood samples from pancreatic cancer patients and cancer-free volunteers

Based on the criterion that the expression level of α4GnT mRNA should exceed the cut-off value of 10.5 for a positive result in this assay, we determined the expression levels of α4GnT mRNA in the mononuclear cell fraction of peripheral blood isolated from 55 pancreatic cancer patients and 70 cancer-free volunteers (Fig. 3).

In pancreatic cancer, 42 (76.4%) of 55 patients examined were positive for this assay, and the expression level of α4GnT mRNA was 37.50 ± 5.44 (mean ± SE). The expression level of α4GnT transcripts was then evaluated by clinicopathological variables including tumor location, stage, venous invasion,

doi: 10.1111/j.1349-7006.2006.00148.x

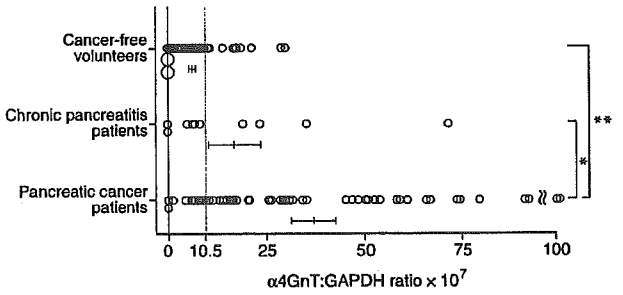

Fig. 3. Scatter plots indicating the expression level of α4GnT mRNA in the mononuclear cell fraction of peripheral blood measured by the quantitative RT-PCR. Small and large circles represent one and 10 individuals, respectively. Horizontal bars indicate mean ± SE. *$P < 0.05$, **$P < 0.001$.

lymphatic invasion and lymph node metastasis determined at subsequent surgical operation. Although the frequency of the positive patients and the expression level of α4GnT seemed to be associated with tumor progression, no significant statistical differences were seen in any clinicopathological variables examined (Table 1).

In addition, the expression level of α4GnT mRNA in the mononuclear cell fraction of blood samples from cancer-free volunteers was determined. Of the 70 cancer-free volunteers examined, 12 (17.1%) volunteers were found to be positive for this assay, but the expression level of α4GnT transcripts was 7.2 ± 0.9, which was significantly lower than that seen in pancreatic cancer patients ($P < 0.001$).

We then tested whether activated lymphocytes express α4GnT mRNA aberrantly by using the Human Blood Fractions MTC Panel, and it was shown that α4GnT mRNA was not detectable in any of the blood fractions examined, including activated lymphocytes.

Detection of α4GnT mRNA in peripheral blood samples from chronic pancreatitis patients

We next measured the expression level of α4GnT in the mononuclear cell fraction of peripheral blood isolated from chronic pancreatitis patients (Fig. 3). Of the 10 patients examined, four (40.0%) were classed as positive by exceeding the defined cutoff of 10.5. However the expression level of α4GnT mRNA was found to be 17.87 ± 6.98, which was again significantly lower than that seen in pancreatic cancer patients ($P < 0.05$). Statistically significant differences between expression levels were not seen between cancer-free volunteers and chronic pancreatitis patients.

Comparison of α4GnT mRNA with well-characterized biomarkers in pancreatic cancer patients

The results of the real-time PCR analysis of α4GnT mRNA expressed in the mononuclear cell fraction of peripheral blood from the pancreatic cancer patients were then compared with the results of enzyme immunoassays for well-characterized biomarkers including CEA, CA19-9, DU-PAN-2 and Span-1. As shown in Table 2, more than 74% of pancreatic patients were positive for either α4GnT or CA19-9, and CEA and DU-PAN-1 were found to less frequently detect pancreatic cancer compared with α4GnT and CA19-9.

Table 1. Frequency of pancreatic cancer patients positive for the α4GnT assay and correlation between expression levels of α4GnT mRNA in peripheral blood mononuclear cells and clinicopathological variables

Variable	Frequency of positive patients†		α4GnT mRNA‡ (mean ± SE)	*P*-value
	n	%		
Tumor location				
Head	25/32	78.1	37.95 ± 7.03	0.9728§
Body and tail	17/23	73.9	36.87 ± 8.78	
Tumor stage				
0	0/1	0	5.290	0.4571¶
II	2/3	66.7	29.44 ± 11.67	
III	7/8	87.5	32.85 ± 8.55	
IV	33/43	76.7	39.68 ± 6.72	
Venous invasion				
Negative	3/5	60.0	29.29 ± 11.20	0.6954§
Positive	17/19	89.5	36.97 ± 10.36	
Lymphatic invasion				
Negative	1/3	33.3	11.81 ± 4.82	0.0606§
Positive	19/21	90.5	38.74 ± 9.44	
Lymph node metastasis				
Negative	5/7	71.4	28.78 ± 9.93	0.8241§
Positive	15/17	88.2	38.09 ± 11.32	

†Expression levels greater than 10.5 were defined as positive.
‡α4GnT:GAPDH mRNA ratios multiplied by 1.0×10^7 are indicated.
§Analyzed using the Mann–Whitney *U*-test. ¶Analyzed using the Kruskal–Wallis test.

We then tested whether a combined assay with α4GnT and another biomarker would detect pancreatic cancer patients more efficiently than the enzyme immunoassays targeting single biomarkers (Table 3). Notably, it was found that more than 86% of pancreatic cancer patients were detected when the α4GnT assay was combined with enzyme immunoassay for CEA, CA19-9, DU-PAN-2 or Span-1. In particular, 96.4% of pancreatic cancer patients were positive for either α4GnT mRNA or Span-1 or both, whereas 71.4% of the patients were positive for Span-1 alone.

Detection of α4GnT protein in resected pancreatic cancer tissues

Transcripts of α4GnT are not detectable in peripheral blood cells, including leukocytes, lymphocytes and monocytes.[17] Thus, it is possible that α4GnT mRNA detected in the mononuclear cell fraction of peripheral blood from pancreatic cancer patients is derived from circulating pancreatic cancer cells expressing α4GnT mRNA. To test this hypothesis, the results of real-time RT-PCR of α4GnT mRNA expressed in the peripheral blood were compared with those of α4GnT protein expressed in 23 cases of the subsequently resected pancreatic cancer tissues by immunohistochemistry with the antiα4GnT antibody I17K. In 19 patients positive for α4GnT transcripts in the peripheral blood, 17 were also positive for α4GnT protein in the resected pancreatic cancer tissues. By contrast, α4GnT protein was not detected in pancreatic cancer tissues of three of four patients who were also negative for the α4GnT mRNA assay. These results indicate a significant association between α4GnT mRNA in the peripheral blood

Table 2. Frequency of pancreatic cancer patients detected using assays for α4GnT mRNA, CEA, CA19-9, DU-PAN-2 and SPan-1

Tumor stage	α4GnT mRNA (> 10.5)		CEA (> 2.5 ng/mL)		CA19-9 (> 37 U/mL)		DU-PAN-2 (> 150 U/mL)		SPan-1 (> 30 U/mL)	
	n	%	*n*	%	*n*	%	*n*	%	*n*	%
0	0/1	0	0/1	0	0/1	0	NE	NE	NE	NE
II	2/3	66.7	0/3	0	0/3	0	0/2	0	0/2	0
III	7/8	87.5	3/8	37.5	6/8	75.0	1/8	12.5	2/7	28.6
IV	33/43	76.7	23/41	56.1	34/42	82.9	16/22	72.7	18/19	94.7
Total	42/55	76.4	26/53	49.1	40/54	74.1	17/32	53.1	20/28	71.4

NE, not evaluated.

Table 3. Frequency of pancreatic cancer patients detected using combined assays†

Biomarker	CEA (> 2.5 ng/mL)		CA19-9 (> 37 U/mL)		DU-PAN-2 (> 150 U/mL)		SPan-1 (> 30 U/mL)	
	n	%	*n*	%	*n*	%	*n*	%
α4GnT mRNA	46/53	86.8	48/54	88.9	30/32	93.8	27/28	96.4
CEA	–	–	43/53	81.1	24/32	75.0	21/28	75.0
CA19-9	–	–	–	–	27/32	84.4	23/28	82.1
DU-PAN-2	–	–	–	–	–	–	21/28	75.0

†Frequency of the patients positive for either or both biomarkers combined is indicated.

and α4GnT protein in pancreatic cancer tissues ($P = 0.0209$), suggesting that α4GnT mRNA detected in patients' peripheral blood is derived from circulating pancreatic cancer cells.

Discussion

α1,4-*N*-Acetylglucosaminyltransferase is a glycosyltransferase that mediates the transfer of GlcNAc with an α1,4-linkage from UDP-GlcNAc to βGal residues, forming α1,4-GlcNAc-capped *O*-glycans.[14] As shown in our previous studies and confirmed here, α4GnT is expressed frequently in pancreatic cancer cells as well as in gastric cancer cells, but not in peripheral blood cells.[15,17] Therefore, we used quantitative RT-PCR to determine the expression level of α4GnT mRNA in tumor cells circulating in the peripheral blood of pancreatic cancer patients. We primarily defined the cut-off value as 10.5 for this assay, based on the ROC curve, and could detect 76.4% of 55 pancreatic cancer patients. The significant correlation between the expression level of α4GnT mRNA in the peripheral blood detected by the RT-PCR assay and α4GnT protein detected in resected pancreatic cancer tissues by immunohistochemistry strongly suggests that α4GnT mRNA detected in the peripheral blood is derived from circulating pancreatic cancer cells. Although 40% of 10 chronic pancreatitis patients and 17.1% of 70 cancer-free volunteers were also positive by this assay, the expression levels of α4GnT mRNA in both groups were significantly lower than those seen in pancreatic cancer patients. These results indicate the clinical utility of real-time RT-PCR targeted to α4GnT mRNA for detection of pancreatic cancer.

The present study also revealed that the location of the pancreatic tumor does not alter the results of the assay (Table 1). It is known that early detection of pancreatic cancer occurring in the tail and body of the pancreas can be particularly difficult because jaundice, which is frequently associated with pancreatic head cancer, is not evident unless the common bile duct is affected by the tumor.[1] Thus, the assay demonstrated here will likely contribute to early detection of pancreatic body and tail cancers that are not associated with jaundice.

In the present study, we have also shown that the expression level of α4GnT mRNA in the peripheral blood from pancreatic cancer patients is elevated in a manner correlated with tumor stage (Table 1), suggesting that the number of cancer cells entering the peripheral blood is increased as the tumor progresses. Most recently, we have shown that α1,4-GlcNAc-capped *O*-glycans secreted from gastric gland mucous cells function as an antibiotic against *H. pylori* infection.[20] The role of these unique *O*-glycans expressed on pancreatic cancer cells remains unknown, and thus further study will be required to address this problem.

There are several biomarkers for pancreatic cancer, including CEA,[5] CA19-9,[6] DU-PAN-2[7,8] and Span-1.[9] Among them, CA19-9 is the most widely used in screening and monitoring of the disease.[21–24] We compared α4GnT with other biomarkers (including CA19-9) and found that the frequency of pancreatic cancer patients detected by α4GnT was much the same as that detected by CA19-9 (Table 2). The same analysis also revealed that DU-PAN-2 and CEA detected pancreatic cancer patients less frequently than α4GnT, CA19-9 and Span-1. It is noteworthy that two of three patients at stage II were positive for α4GnT mRNA, suggesting the possible usefulness of α4GnT mRNA for the early detection of pancreatic cancer. Further study on a larger number of patients with stages 0, I and II will be required to prove this possibility.

The present study demonstrated that the frequency of pancreatic cancer patients detected using enzyme immunoassays for CEA, CA19-9, DU-PAN-2 and Span-1 was increased substantially when combined with the α4GnT assay (Table 3). It is generally accepted that the quantitative RT-PCR assay requires much time and cost compared with enzyme immunoassay.

doi: 10.1111/j.1349-7006.2006.00148.x

However, the combined assay with α4GnT mRNA can detect pancreatic cancer patients more efficiently when compared with the enzyme immunoassays targeting single biomarkers.

The present study also demonstrated that the expression levels of α4GnT mRNA were elevated in 40% of chronic pancreatitis patients and 17% of cancer-free volunteers, albeit at much lower levels than those of pancreatic cancer patients. Previously, we showed that significant amounts α4GnT mRNA were detected in patients with *H. pylori* infection or chronic gastroduodenal ulcers.[17] It has been reported that unexpected genes such as α-fetoprotein are transcribed in lymphocytes when they are activated,[25] suggesting the possibility that α4GnT mRNA might be induced in the activated lymphocytes circulating in the *H. pylori*-infected patients. However, as shown previously[17] and further confirmed here, we have demonstrated that α4GnT mRNA is not detectable in activated lymphocytes or resting lymphocytes. By contrast, we have also reported that extensive biopsy of the gastric mucosa results in elevation of the α4GnT mRNA level in peripheral blood.[26] These results combined suggest that the gastric gland mucous cells expressing α4GnT mRNA enter the bloodstream through the injured sites of gastric mucosa caused by inflammation or biopsy. Considering the high incidence of *H. pylori* infection in individuals over 40 years of age in Japan,[27,28] α4GnT mRNA detected in the cancer-free volunteers is most likely derived from gastric gland mucous cells that have entered the peripheral blood through injured sites of the gastric mucosa caused by *H. pylori* infection. We previously demonstrated that α4GnT mRNA is not detected in the peripheral blood of healthy volunteers without *H. pylori* infection.[17] Similary, it may also be possible that α4GnT mRNA detected in the chronic pancreatitis patients originated from the α4GnT-positive pancreatic duct epithelia entering the blood circulation, because the disruption of pancreatic ducts could occur in chronic pancreatitis (Fig. 1c).[29] Further studies will be of significance to identify the cells that elevate the α4GnT mRNA level in the peripheral blood of these non-cancerous patients.

Recently we demonstrated that α4GnT is expressed not only in pancreatic carcinoma cells but also in biliary tract carcinoma cells that produce α1,4-GlcNAc-capped *O*-glycans.[15] Thus, the α4GnT assay will also be applicable to the detection of patients with biliary tract cancers. We have shown that α4GnT mRNA was detected in three of five patients with biliary tract cancer.[17] It is of great significance to determine the clinical utility of the α4GnT assay for diagnosis of biliary tract cancer as well.

Collectively, our results obtained in the present study indicate that quantitative analysis of α4GnT mRNA expressed in the peripheral blood allowed us to detect pancreatic cancer cells expressing α1,4-GlcNAc-capped *O*-glycans. In order to clarify the clinical contribution of this assay system, prospective controlled trials are needed in the screening, diagnosis and monitoring of pancreatic cancer patients.

Acknowledgments

This study was supported by Grant-in-Aids for 3rd Term Comprehensive Control Research for Cancer from the Ministry of Health, Labor and Welfare of Japan and Scientific Research on Priority Areas 14030032 and 14082201 from the Ministry of Education, Culture, Sports, Science and Technology of Japan (to JN), and by NIH Grant CA48737 from the National Institutes of Health (to MF). The authors thank Drs Tsutomu Katsuyama and Fukuto Maruta for encouragement during this work. We are also grateful to Dr Elise Lamar for critical reading of the manuscript.

References

1 Warshaw AL, Castillo CF. Pancreatic carcinoma. *N Engl J Med* 1992; **326**: 455–65.
2 Wagner M, Redaelli C, Lietz M *et al.* Curative resection is the single most important factor determining outcome in patients with pancreatic adenocarcinoma. *Br J Surg* 2004; **91**: 586–94.
3 Kuroki T, Tomioka T, Tajima Y *et al.* Detection of the pancreas-specific gene in the peripheral blood of patients with pancreatic carcinoma. *Br J Cancer* 1999; **81**: 350–3.
4 Iacobuzio-Donahue CA, Maitra A, Shen-Ong GL *et al.* Discovery of novel tumor markers of pancreatic cancer using global gene expression technology. *Am J Pathol* 2002; **160**: 1239–49.
5 Gold P, Freedman S. Demonstration of tumor-specific antigens in human colonic carcinoma by immunological tolerance and absorption techniques. *J Exp Med* 1965; **121**: 439–62.
6 Koprowski H, Steplewski Z, Mitchell K, Herlyn M, Herlyn D, Fuhrer P. Colorectal carcinoma antigens detected by hybridoma antibodies. *Somatic Cell Genet* 1979; **5**: 957–72.
7 Metzgar RS, Rodriguez N, Finn OJ *et al.* Detection of a pancreatic cancer-associated antigen (DU-PAN-2 antigen) in serum and ascites of patients with adenocarcinoma. *Proc Natl Acad Sci USA* 1984; **81**: 5242–6.
8 Haviland AE, Borowitz MJ, Killenberg PG, Lan MS, Metzgar RS. Detection of an oncofetal antigen (DU-PAN-2) in sera of patients with non-malignant hepatobiliary disease and hepatomas. *Int J Cancer* 1988; **41**: 789–93.
9 Kiriyama S, Hayakawa T, Kondo T *et al.* Usefulness of a new tumor marker, span-1, for the diagnosis of pancreatic cancer. *Cancer* 1990; **65**: 1557–61.
10 Koopmann J, Zhang Z, White N *et al.* Serum diagnosis of pancreatic adenocarcinoma using surface-enhanced laser desorption and ionization mass spectrometry. *Clin Cancer Res* 2004; **10**: 860–8.
11 Rosewicz S, Wiedenmann B. Pancreatic carcinoma. *Lancet* 1997; **349**: 485–9.
12 Nakamura N, Ota H, Katsuyama T *et al.* Histochemical reactivity of normal, metaplastic, and neoplastic tissues to α-linked *N*-acetylglucosamine residue-specific monoclonal antibody HIK1083. *J Histochem Cytochem* 1998; **46**: 793–801.
13 Hruban RH, Goggins M, Parsons J, Kern SE. Progression model for pancreatic cancer. *Clin Cancer Res* 2000; **6**: 1835–9.
14 Nakayama J, Yeh J-C, Misra AK, Ito S, Katsuyama T, Fukuda M. Expression cloning of a human α1,4-*N*-acetylglucosaminyltransferase that forms GlcNAcα1→4Galβ→R, a glycan specifically expressed in the gastric gland mucous cell-type mucin. *Proc Natl Acad Sci USA* 1999; **96**: 8991–6.
15 Nakajima K, Ota H, Zhang MX *et al.* Expression of gastric gland mucous cell-type mucin in normal and neoplastic human tissues. *J Histochem Cytochem* 2003; **51**: 1689–98.
16 Zhang MX, Nakayama J, Hidaka E *et al.* Immunohistochemical demonstration of α1,4-N-acetylglucosaminyltransferase that forms GlcNAcα1,4Galβ residues in human gastrointestinal mucosa. *J Histochem Cytochem* 2001; **49**: 587–96.
17 Shimizu F, Nakayama J, Ishizone S *et al.* Usefulness of the real-time reverse transcription–polymerase chain reaction assay targeted to α1,4-*N*-acetylglucosaminyltransferase for the detection of gastric cancer. *Lab Invest* 2003; **83**: 187–97.
18 Sobin LH, Wittekind C, eds. *TNM Classification of Malignant Tumours*, 5th edn. New York, NY: John Wiley-Liss, 1997.
19 Machida E, Nakayama J, Amano J, Fukuda M. Clinicopathological

significance of core2 β1,6-*N*-acetylglucosaminyltransferase messenger RNA expressed in the pulmonary adenocarcinoma determined by *in situ* hybridization. *Cancer Res* 2001; **61**: 2226–31.
20 Kawakubo M, Ito Y, Okimura Y *et al.* Natural antibiotic function of a human gastric mucin against *Helicobacter pylori* infection. *Science* 2004; **305**: 1003–6.
21 Ziske C, Schlie C, Gorschluter M *et al.* Prognostic value of CA19-9 levels in patients with inoperable adenocarcinoma of the pancreas treated with gemcitabine. *Br J Cancer* 2003; **89**: 1413–17.
22 Tanaka N, Okada S, Ueno H, Okusaka T, Ikeda M. The usefulness of serial changes in serum CA19-9 levels in the diagnosis of pancreatic cancer. *Pancreas* 2000; **20**: 378–81.
23 Koopmann J, Buckhaults P, Brown DA *et al.* Serum macrophage inhibitory cytokine 1 as a marker of pancreatic and other periampullary cancers. *Clin Cancer Res* 2004; **10**: 2386–92.
24 Nakao A, Oshima K, Nomoto S *et al.* Clinical usefulness of CA19-9 in pancreatic carcinoma. *Semin Surg Oncol* 1998; **15**: 15–22.
25 Lafarge-Frayssinet C, Torres JM, Frain M, Uriel J. α-Fetoprotein gene expression in human lymphoblastoid cells and in PHA-stimulated normal T-lymphocytes. *Biochem Biophys Res Commun* 1989; **159**: 112–18.
26 Shimizu F, Nakayama J, Sugiyama A, Kawasaki S, Katsuyama T. Gastric gland mucous cells circulate in peripheral blood after endoscopic biopsy of the gastric mucosa. *Am J Gastroenterol* 2000; **95**: 3017–18.
27 Asaka M, Kimura T, Kudo M *et al.* Relationship of *Helicobacter pylori* to serum pepsinogens in an asymptomatic Japanese population. *Gastroenterology* 1992; **102**: 760–6.
28 Matsuhisa TM, Yamada NY, Kato SK, Matsukura NM. *Helicobacter pylori* infection, mucosal atrophy and intestinal metaplasia in Asian populations: A comparative study in age-, gender- and endoscopic diagnosis-matched subjects. *Helicobacter* 2003; **8**: 29–35.
29 Oertel JE, Oertel YC, Heffess CS. Pancreas. In: Sternberg SS, ed. *Diagnositic Surgical Pathology*. New York: Raven Press, 1994; 1419–57.

doi: 10.1111/j.1349-7006.2006.00148.x

Pathology International 2006; 56: 95–100 doi:10.1111/j.1440-1827.2006.01930.x

Case Report

Female adnexal tumor of probable wolffian origin: Morphological, immunohistochemical, and ultrastructural study with *c-kit* gene analysis

Oi Harada,[1] Hiroyoshi Ota,[2] Kimiyo Takagi,[3] Hiroyuki Matsuura,[4] Eiko Hidaka[5] and Jun Nakayama[1]

Departments of [1]Pathology, [2]Biomedical Laboratory Sciences and [5]Laboratory Medicine, Shinshu University School of Medicine, Matsumoto and Departments of [3]Obstetrics and Gynecology and [4]Laboratory Medicine, Iiyama Red Cross Hospital, Iiyama, Japan

Female adnexal tumors of probable wolffian origin (FATWO) are rare neoplasms believed to originate from mesonephric (wolffian) remnants. Rarity and variable location of FATWO make the diagnosis difficult. Although most cases follow a benign clinical course, approximately 10% of them either recur or metastasize and are thought to be resistant to chemoradiation therapy. In 2004, imatinib therapy, a tyrosine kinase inhibitor known to be effective against gastrointestinal stromal tumors, was reported to be effective also in a case of KIT-positive FATWO. However, *c-kit* gene mutations in FATWO have never been studied. Herein is reported the case of a 50-year-old Japanese woman with FATWO arising in the right paratubal site. The tumor had typical characteristics of FATWO in both morphology and immunohistochemistry. KIT protein was diffusely and weakly expressed, but DNA analysis revealed no mutational change in exon 9 or 11 of the *c-kit* gene. It is believed that accumulation of such genetic data of FATWO are essential from a therapeutic standpoint, although the present case had no mutation. In addition, the cytological features of this rare tumor are presented, which have not been described previously.

Key words: electron microscopy, female adnexal tumor of probable wolffian origin, GIST, imatinib, immunohistochemistry, KIT, touch imprint cytology

Female adnexal tumors of probable wolffian origin (FATWO) are rare gynecological tumors. They were first reported in 1973 by Kariminejad and Scully[1] and fewer than 80 cases have been reported so far. They are distinctive epithelial neoplasm and are believed to arise from the remnants of the mesonephric duct.[2,3] However, owing to their rarity and variable location, the diagnosis of FATWO may occasionally be difficult and challenging.[4]

Correspondence: Oi Harada, MD, Department of Pathology, Shinshu University School of Medicine, 3-1-1 Asahi, Matsumoto, Nagano 390-8621, Japan. Email: oharada@hsp.md.shinshu-u.ac.jp

Received 16 August 2005. Accepted for publication 18 October 2005.

Although most FATWO behave in a benign fashion, malignant cases do exist.[3,5–7] In such malignant cases, the effectiveness of adjuvant chemotherapy or radiation therapy is thought to be questionable.[8] In 2004 Steed *et al.* reported on a malignant FATWO case that had positive immunoreactivity for KIT protein (CD117).[7] Before operation, imatinib (formerly STI571), a competitive tyrosine kinase inhibitor, was prescribed using a similar protocol to the treatment of gastrointestinal stromal tumors (GIST), and the tumor responded favorably. However, it was not certain whether *c-kit* gene mutations of the tumor contributed to the favorable response to the therapy, because genetic analysis was not performed.

Here we present the case of a KIT-positive FATWO arising in a Japanese middle-aged woman. We analyze the *c-kit* gene status, and also describe cytological features on intraoperative touch imprinting cytology (TIC) as well as histological, immunohistochemical, and ultrastructural findings.

CASE REPORT

A 50-year-old gravida 0 parity 0 Japanese woman presented to hospital because of painless lower abdominal swelling. She was otherwise well and had no significant past history. Her menstruation cycle had been irregular, and the last menstruation was 20 days before her consultation and lasted for 8 days. Ultrasonic examination and magnetic resonance imaging (MRI) revealed a leiomyomatous uterus and a right paratubal solid mass lesion (Fig. 1). The serum level of cancer antigen 125 (CA125) was 95.3 U/mL (normal value: <35.0 U/mL). Subsequently, the patient underwent total abdominal hysterectomy and right salpingo-oophorectomy. At operation, an approximately 50 mm tumorous mass was found beside the right fallopian tube, which was stretched and mildly dilated because of the mass. No metastatic or disseminated tumor was observed. The mass had no adhe-

sion to surrounding tissue and was easily detached from the tube. The contralateral tube and bilateral ovaries appeared to be normal. There were also multiple leiomyomatous nodules in the uterus. No other abnormality was found at operation including ascites and pelvic endometriosis. She was well and continued to be free of the disease 11 months after the operation without further treatment. The serum level of CA125 decreased to 13.9 U/mL.

PATHOLOGICAL FINDINGS

Gross and microscopic findings

The tumor was fragile and thus was received fragmented. It measured approximately 50 × 45 × 30 mm. Cut surface of the tumor revealed a white to yellow-colored solid mass without apparent cystic area. Neither hemorrhagic nor necrotic region was observed.

On intraoperative TIC many tubular or trabecular arrangements of tumor cells with loosely aggregated area were seen (Fig. 2a). Necrotic background was not observed. The tumor cells were short columnar to oval shaped, and the cell borders were not clearly defined. Each cell had a round nucleus with fine granular chromatin and scant pale cytoplasm. Nuclear atypia was minimum and one or two nucleoli were occasionally observed (Fig. 2b). These findings did not fit the definite malignancy, although the histological examination of intraoperative frozen section could not rule out the possibility of adenocarcinoma.

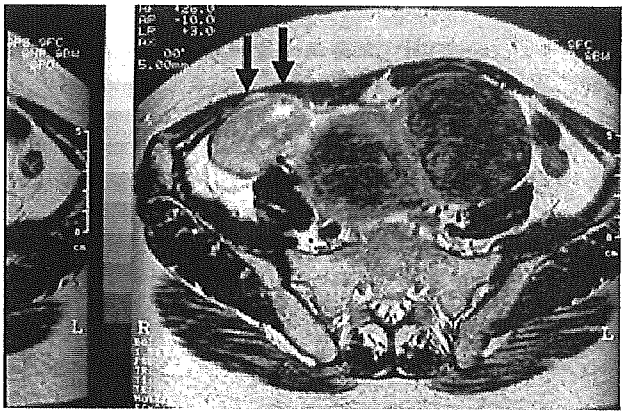

Figure 1 T2-weighted magnetic resonance imaging showing a right paratubal mass (arrows).

Histological examination of formalin-fixed tissue revealed neoplastic cells arranged in tubular and solid fashions with a sieve-like pattern, which displayed clusters of small-sized cysts lined by the neoplastic cells (Fig. 3a). Periodic acid–Schiff (PAS) stain highlighted the tubular pattern and distinct basement membrane (Fig. 3b). Mitoses were rare, numbering less than 1 per 10 high-power fields (HPF). Cytoplasmic glycogen, mucin production, and squamous cell differentiation were not observed. Although the fallopian tube was partially dilated because of the tumor's physical compression, no neoplastic involvement was observed. All of the myomatous nodules in the uterus had histological features of conventional leiomyoma without nuclear atypia or mitoses.

Immunohistochemical findings

Immunohistochemical analyses were performed using Envision+ (DakoCytomation, Glostrup, Denmark) with a 3,3′-diaminobenzidine tetrahydrochloride as a chromogen. The primary antibodies used in the present study are listed in Table 1.

The tumor cells were diffusely and strongly positive for vimentin. Low-molecular-weight cytokeratin, cytokeratin (CK) 7, and calretinin were also expressed in most tumor cells. In contrast, only focal staining for CD10 and diffuse weak staining for KIT protein (CD117, Fig. 4) were observed.

Table 1 List of primary antibodies used

Anti-	Clone	Source	Dilution	Retrieval
Vimentin	Clone V9	DakoCytomation, Glostrup, Denmark	1:100	Microwave
α-Smooth muscle actin	Clone 1A4	DakoCytomation	1:50	Microwave
Low-molecular-weight cytokeratin	Clone CAM5.2	Becton Dickinson, Franklin Lakes, NJ, USA	1:2	Microwave
High-molecular-weight cytokeratin	Clone 34betaE12	DakoCytomation	1:40	Microwave
Cytokeratin 7	Clone OV-TL 12/30	DakoCytomation	1:30	Microwave
Cytokeratin 20	Clone Ks20.8	DakoCytomation	1:30	Microwave
Epithelial membrane antigen	Clone GP1.4	Novocastra, Newcastle upon Tyne, UK	1:100	Microwave
Calretinin	Clone DAK Calret1	DakoCytomation	1:30	Microwave
Inhibin	Clone R1	DakoCytomation	1:30	Microwave
CD34	Clone QBEnd10	Immunoteck, Marseilles, France	1:100	Microwave
CD10	Clone 56C6	Novocastra	1:20	Microwave
Estrogen receptor	Clone 6F11	Ventana, Tuscon, AZ, USA	×1 (prediluted)	Microwave
Progesterone receptor	Clone 1A6	Ventana	×1	Microwave
c-kit (CD117)	Code A4502, rabbit polyclonal	DakoCytomation	×20	Microwave
Ki-67 antigen	Clone MIB-1	DakoCytomation	1:40	Microwave

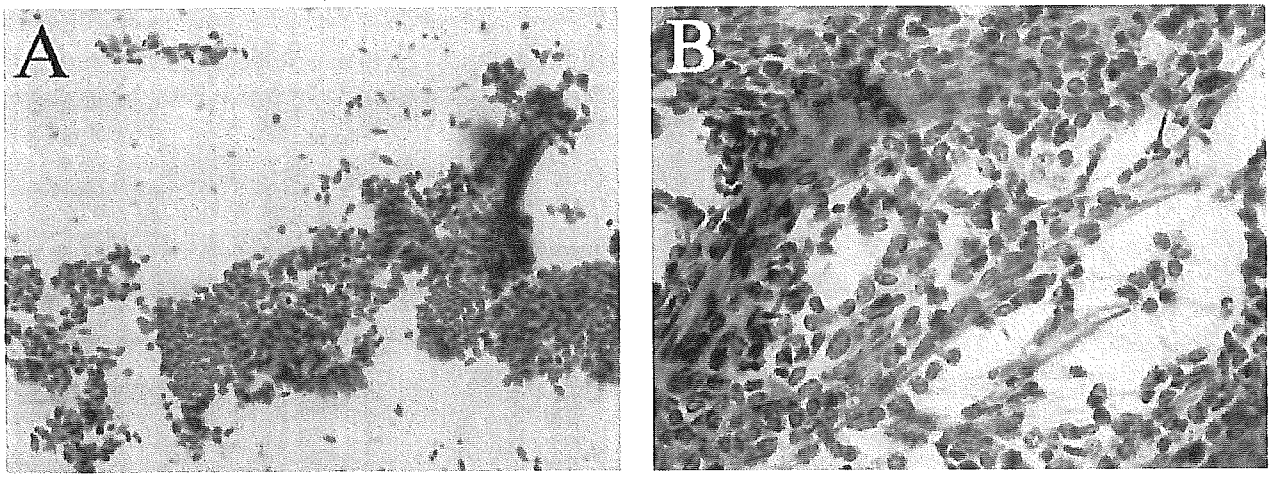

Figure 2 Touch imprinting cytology of the tumor cells (Papanicolaou stain). (**A**) Tubular to trabecular arrangement is observed. (**B**) Tumor cells possess a round nucleus with fine granular chromatin. Nuclear atypia was minimum.

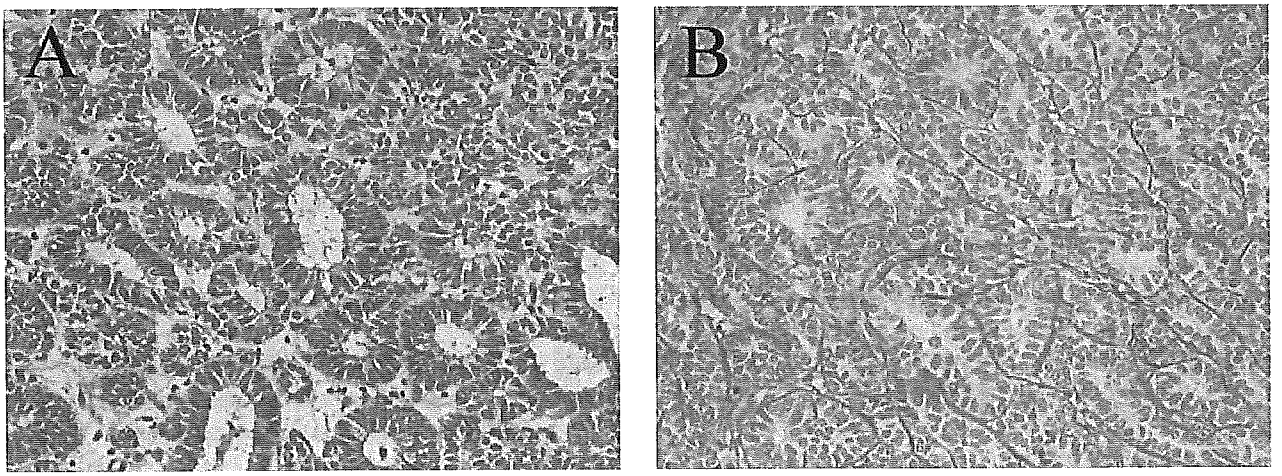

Figure 3 (**A**) Female adnexal tumor of probable wolffian origin (FATWO) showing a sieve-like pattern of growth (HE). (**B**) PAS staining highlighted the basement membrane (AB-PAS).

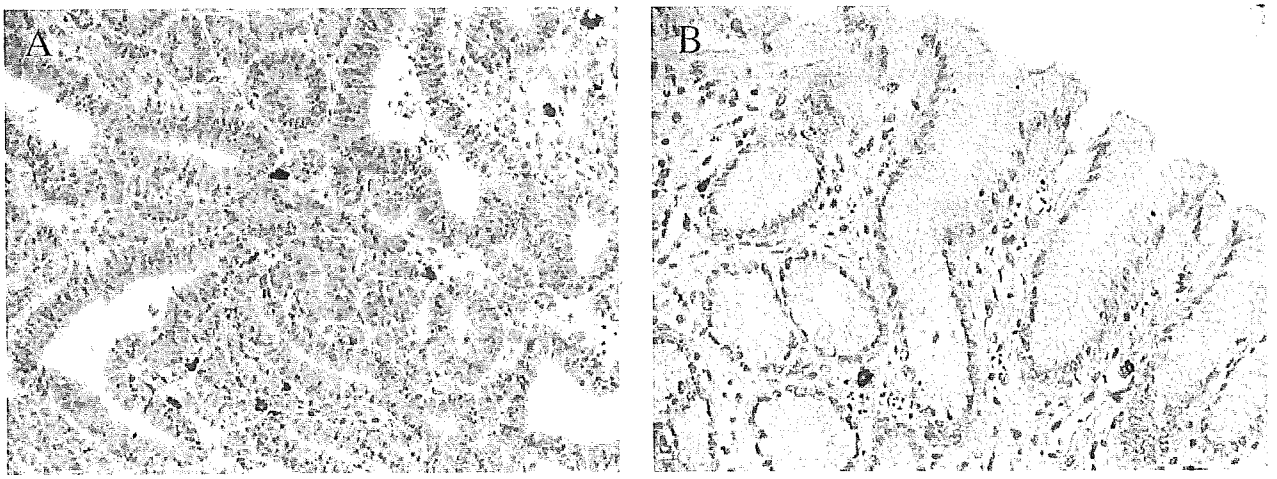

Figure 4 Immunohistochemistry for KIT. (**A**) The tumor cells are weakly positive, while mast cells are strongly positive. (**B**) Background staining was negligible (gastric mucosa).

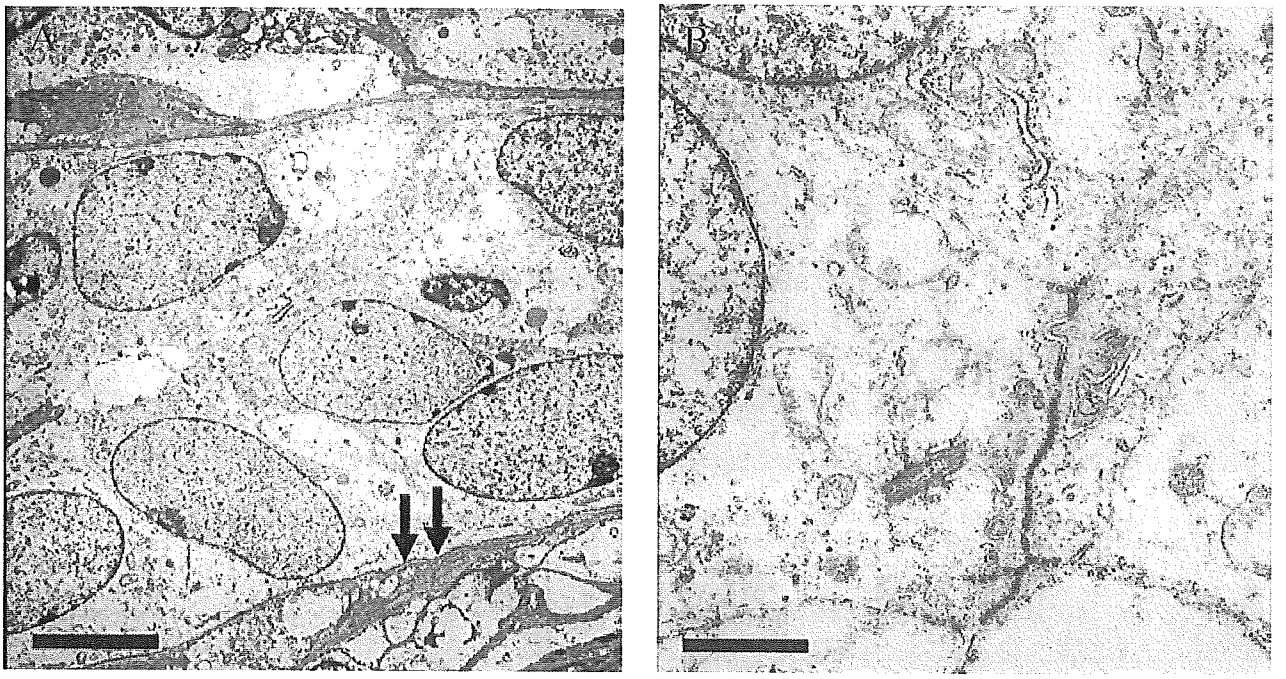

Figure 5 Ultrastructure of the tumor cells. (**A**) Distinct basal lamina (arrows) and sparse organelles are observed. Scale bar, 5 μm. (**B**) Intercellular desmosomal junction is prominent. Scale bar, 1 μm.

Tumor cells were negative for α-smooth muscle actin, high-molecular-weight cytokeratin, CK20, epithelial membrane antigen, inhibin, CD34, estrogen receptor, and progesterone receptor. The positive rate for Ki-67 proliferating cell marker was <3% at most.

Ultrastructural findings

For ultrastructural study, small pieces of the tumor tissue were fixed in 2.5% glutaraldehyde in 0.1 mol/L phosphate buffer pH 7.4 (PB) overnight, contrasted in 1% osmium tetroxide and embedded in epoxy resin. The ultrathin sections were stained with uranyl acetate and lead citrate, and examined under a JEM1230 transmission electron microscope (JEOL, Tokyo, Japan).

Electron microscopic examination revealed distinct basal laminae and desmosomal junctions between tumor cells (Fig. 5). Cytoplasmic organelles were not well-developed, that is, there were only few lysosomes, endoplasmic reticulums, mitochondria, and lipid droplets. Neither cilia nor secretory granules were observed.

Molecular study for *c-kit* gene

Genomic DNA was extracted from alcohol-fixed TIC specimens by standard phenol-chloroform-isoamylalcohol extraction methods. A polymerase chain reaction (PCR) amplification of exon 9 and 11 of the *c-kit* gene was performed using a previously published procedure with some modification.[9,10] The primer sets used for PCR were as follows: exon 9 forward primer, 5′-atgctctgcttctgtactgcc-3′; exon 9 reverse primer, 5′-cagagcctaaacatcccctta-3′; exon 11 forward primer, 5′-ccagagtgctctaatgactg-3′; exon 11 reverse primer, 5′-agcccctgtttcatactgacc-3′. The PCR products were directly sequenced using an ABI PRISM 310 genetic analyzer (Applied Biosystems, Foster City, CA, USA) according to the manufacturer's protocol.

Sequencing analysis of exon 9 and 11 of the *c-kit* gene revealed no mutational change (data not shown).

DISCUSSION

We report herein the case of a 50-year-old Japanese woman with FATWO arising in the right paratubal site, and have described the cytological, histological, immunohistochemical, and ultrastructural findings, as well as *c-kit* gene status. The morphological and immunohistochemical findings observed in the present case were consistent with those of previously reported FATWO, namely characteristic tubular or sieve-like cystic patterns of epithelial cells in histology, immunohistochemical positivity for vimentin, low-molecular-weight cytokeratin, CK7, and calretinin, and the presence of thick basal laminae and prominent desmosomes in ultrastruc-

ture.[2,3,5,11,12] In addition, the tumor cells had weak positivity for KIT protein.

Because the effectiveness of imatinib therapy in KIT-positive FATWO cases has been reported,[7] we tried to determine whether the tumor had *c-kit* gene abnormalities. In GIST, exon 11 of the *c-kit* gene (juxtamembrane domain) has been shown to be the predominantly mutated lesion. Mutations of exon 9 (extracellular domain) have also been found in a small number of cases. In contrast, additional exon 13 and 17 mutations had been reported but they are very rare.[10,13,14] Hence we performed PCR and sequencing analyses for exon 9 and 11 of the *c-kit* gene. To our knowledge, this is the first FATWO case in which *c-kit* gene analysis has been performed. However, sequencing analysis revealed no mutation in either exon 9 or 11. It still remains unclear whether *c-kit* gene mutations are essential to FATWO.

Recently, platelet-derived growth factor receptor-α (PDGFRA) has been shown to be mutated in KIT mutation-negative GIST,[15] although the frequencies of mutation are much lower than those of KIT (95% vs 5%).[13] KIT and PDGFRA display an extensive structural homology,[14] and PDGFRA mutations in GIST have been reported to be present in exon 18 (kinase activation loop) and in exon 12 (juxtamembrane domain).[13,15] Thus the possibility of PDGFRA mutations in FATWO remains because KIT and PDGFRA mutations are mutually exclusive in GIST. Further case studies with gene analyses are needed to clarify this issue.

Fortunately the tumor has not recurred in the follow-up period of 11 months. However, it is difficult to predict the biological behavior of FATWO because it has been reported that tumors with minimal nuclear atypia and a very low mitotic rate might also recur.[8] It is also uncertain at this time whether the patient would have a favorable response to imatinib in the case of tumor recurrence.

As well as the KIT analysis, cytological examination was also performed in the present case, using TIC at intraoperative evaluation. To the best of our knowledge, this is the first case showing cytology of FATWO. The TIC results did not fit the definite malignancy and showed consistent features with previously described histological features of FATWO, but other diseases such as pelvic endometriosis or endometrioid borderline tumors should also be considered from TIC findings alone. However, considering that the examination of intraoperative frozen section could not rule out the possibility of adenocarcinoma, the TIC examination might be potentially useful for the differential diagnosis as described here, and also for diagnosis of FATWO.

Differential diagnosis in histology includes Sertoli-Leydig cell tumor, granulosa cell tumor, and endometrioid carcinoma.[2,3] Of these, Sertoli–Leydig cell tumors may bear a strong morphological resemblance to FATWO.[2,4] The presence of a sieve-like pattern, the absence of Leydig cells, and the lack of immunoreactivity for inhibin may be useful for diagnosis of FATWO.[12] In addition, Sertoli–Leydig cell tumors have not been reported in the paratubal site or in the broad ligament. Granulosa cell tumors are also important for differential diagnosis because of their microfollicular and/or trabecular patterns that occasionally mimic FATWO. However, their cytological appearance is characteristic and quite different from those of FATWO. Well-differentiated endometrioid carcinoma can arise in the fallopian tubes and may possibly mimic FATWO in morphology.[3] Tumor cells in endometrioid carcinoma, however, occasionally present focal squamous cell differentiation, intraluminal mucin, prominent nuclear atypia and mitoses. Such histopathological findings have not been demonstrated in FATWO cases. TIC examination might be useful for differential diagnosis, as described here. Metastatic endometrioid carcinoma from the ovary also must be considered, especially in spindle cell-rich form,[16] but the clue to differential diagnosis is similar.

In summary, we report herein a FATWO case that was immunohistochemically KIT positive but which had no mutational change in exons 9 or 11 of the *c-kit* gene. This is the first FATWO case in which *c-kit* gene analyses were performed, and we believe that further case studies are needed to determine the frequency of *c-kit* gene mutations in FATWO. Furthermore, confirmations of effectiveness of imatinib and its mechanism should also be investigated in order to establish the therapeutic tactics for FATWO.

ACKNOWLEDGMENT

This work was supported in part by Grant-in-Aid for Scientific Research B-15390115 from the Japan Society for the Promotion of Science.

REFERENCES

1 Kariminejad MH, Scully RE. Female adnexal tumor of probable Wolffian origin. A distinctive pathologic entity. *Cancer* 1973; **31**: 671–77.
2 Li CC, Qian ZR, Hirokawa M *et al.* Expression of adhesion molecules and Ki-67 in female adnexal tumor of probable Wolffian origin (FATWO): Report of two cases and review of the literature. *APMIS* 2004; **112**: 390–98.
3 Tavassoli FA, Devilee P, eds. *World Health Organization Classification of Tumours. Pathology and Genetics of Tumours of the Breast and Female Genital Organs.* Lyon: IARC Press, 2003; 212–13.
4 Devouassoux-Shisheboran M, Silver SA, Tavassoli FA. Wolffian adnexal tumor, so-called female adnexal tumor of probable Wolffian origin (FATWO): Immunohistochemical evidence in support of a Wolffian origin. *Hum Pathol* 1999; **30**: 856–63.
5 Sheyn I, Mira JL, Bejarano PA, Husseinzadeh N. Metastatic female adnexal tumor of probable Wolffian origin: A case report and review of the literature. *Arch Pathol Lab Med* 2000; **124**: 431–34.

6 Atallah D, Rouzier R, Voutsadakis I *et al.* Malignant female adnexal tumor of probable wolffian origin relapsing after pregnancy. *Gynecol Oncol* 2004; **95**: 402–4.
7 Steed H, Oza A, Chapman WB, Yaron M, De Petrillo D. Female adnexal tumor of probable wolffian origin: A clinicopathological case report and a possible new treatment. *Int J Gynecol Cancer* 2004; **14**: 546–50.
8 Ramirez PT, Wolf JK, Malpica A, Deavers MT, Liu J, Broaddus R. Wolffian duct tumors: Case reports and review of the literature. *Gynecol Oncol* 2002; **86**: 225–30.
9 Lasota J, Jasinski M, Sarlomo-Rikala M, Miettinen M. Mutations in exon 11 of KIT occur preferentially in malignant versus benign gastrointestinal stromal tumors and do not occur in leiomyomas or leiomyosarcomas. *Am J Pathol* 1999; **154**: 53–60.
10 Miettinen M, Sobin LH, Lasota J. Gastrointestinal stromal tumors of the stomach: A clinicopathologic, immunohistochemical, and molecular genetic study of 1765 cases with long-term follow-up. *Am J Surg Pathol* 2005; **29**: 52–68.
11 Rahilly MA, Williams AR, Krausz T, al Natussi A. Female adnexal tumour of probable Wolffian origin: A clinicopathological and immunohistochemical study of three cases. *Histopathology* 1995; **26**: 69–74.
12 Tiltman AJ, Allard U. Female adnexal tumours of probable Wolffian origin: An immunohistochemical study comparing tumours, mesonephric remnants and paramesonephric derivatives. *Histopathology* 2001; **38**: 237–42.
13 Heinrich MC, Corless CL, Demetri GD *et al.* Kinase mutations and imatinib response in patients with metastatic gastrointestinal stromal tumor. *J Clin Oncol* 2003; **21**: 4342–49.
14 Lasota J, Dansonka-Mieszkowska A, Sobin LH, Miettinen M. A great majority of GISTs with PDGFRA mutations represent gastric tumors of low or no malignant potential. *Lab Invest* 2004; **84**: 874–83.
15 Heinrich MC, Corless CL, Duensing A *et al.* PDGFRA activating mutations in gastrointestinal stromal tumors. *Science* 2003; **299**: 708–10.
16 Tornos C, Silva EG, Ordonez NG, Gershenson DM, Young RH, Scully RE. Endometrioid carcinoma of the ovary with a prominent spindle-cell component, a source of diagnostic confusion. A report of 14 cases. *Am J Surg Pathol* 1995; **19**: 1343–53.

Pathology International 2005; **55**: 510–513

Case Report

Malignant myoepithelioma (myoepithelial carcinoma) of soft tissue

Oi Harada,[1] Hiroyoshi Ota[2] and Jun Nakayama[1]

Departments of [1]Pathology and [2]Biomedical Laboratory Sciences, Shinshu University School of Medicine, Matsumoto, Nagano, Japan

Malignant myoepithelioma of soft tissue is extremely rare. Presented herein is a case arising in a 17-year-old man. The tumor was initially noticed as a painless deep soft-tissue mass in the right forearm when the patient was aged 3 years. Thereafter, it grew without remarkable symptoms, such as pain or tenderness, until his visit to the hospital because of swelling of his forearm when he was 17 years old. An excisional biopsy specimen disclosed an invasive tumor exhibiting a lobular architecture. The tumor cells were arranged in a reticular and/or trabecular fashion with a myxoid background, and nuclear atypia was evident. Mitoses and tumor necrosis were also observed. Immunohistochemically, S-100 protein and epithelial markers were diffusely positive. Faint intercellular junctions and basal laminae were identified by electronmicroscopy. On the basis of these findings, the tumor was diagnosed as a malignant myoepithelioma of soft tissue. Six months later, multiple lung metastases were observed, and an open biopsy revealed a neoplasm displaying the same histological feature as the previously biopsied specimens. The patient died of his disease 18 months after the lung biopsy. Malignant myoepithelioma shoud be kept in mind in diagnosis of deep soft-tissue tumors with epithelioid features.

Key words: electron microscopy, immunohistochemistry, lung metastasis, malignant myoepithelioma, mixed tumor, soft tissue

Myoepithelial tumors of the soft tissue are very rare,[1] although they are relatively common in the skin and salivary glands, especially in the parotid glands.[2] The malignant form is still rarer, and only a small number of cases have been reported. Here we describe a case of malignant myoepithelioma (myoepithelial carcinoma) of soft tissue in the forearm. This tumor had preexisted as a deep soft-tissue mass for approximately 14 years, and it metastasized to the lung 6 months after the initial resection.

Correspondence: Oi Harada, MD, Department of Pathology, Shinshu University School of Medicine, 3-1-1 Asahi, Matusumoto, Nagano 390-8621, Japan. Email: oharada@hsp.md.shinshu-u.ac.jp

Received 20 October 2004. Accepted for publication 7 April 2005.

CLINICAL SUMMARY

A 17-year-old man was referred to Shinshu University Hospital because of a right forearm swelling. He and his parents had initially become aware of the mass when he was a 3-year-old boy, and it had been growing slowly until his visit to the hospital, although he had experienced no pain during this progression. Magnetic resonance imaging (MRI) revealed a soft-tissue mass with no attachment to the skin (Fig. 1). A local excisional biopsy was performed. After a follow-up period of 6 months, multiple lung metastases were observed, and an open lung biopsy was carried out. Respiratory failure developed gradually, and the patient died of his disease 18 months after the lung biopsy. An autopsy was not performed.

PATHOLOGICAL FINDINGS

The primary tumor was lobulated, with a mixed solid and reticular or trabecular architecture (Fig. 2a). Apparent infiltrative growth pattern was also observed (Fig. 2b). It was composed of epithelioid, plasmacytoid, and/or spindle cells, usually with an eosinophilic cytoplasm (Fig. 2c,d), in a variably myxoid or hyalinized stroma that was positive for alcian blue. As in MRI, an attachment to the skin was not demonstrated. Neither ductal nor sarcomatous components were observed. Some tumor cells had a clear cytoplasm. The majority of the tumor cells had enlarged nuclei with distinct atypia and/or nucleoli, and occasional mitotic figures were identified (2–3/10 high-power fields (HPF)). Vascular invasion, and tumor necrosis were also observed (Fig. 2e,f).

Immunohistochemical examination was performed on formalin-fixed, paraffin-embedded tissue using antibodies against the following antigens with microwave antigen retrieval: vimentin (clone V9, DakoCytomation, Glostrup, Denmark, 1:100), α-smooth muscle actin (SMA; clone 1A4, DakoCytomation, 1:50), desmin (clone D33, DakoCytoma-